

1 **Tropospheric ozonesonde profiles at long-term U.S. monitoring sites: 2. Links between**
2 **Trinidad Head, CA, profile clusters and inland surface ozone measurements**

3 Ryan M. Stauffer^{1,2}, Anne M. Thompson^{2,3}, Samuel J. Oltmans^{4,5}, Bryan J. Johnson⁵

4

5 ¹Earth System Science Interdisciplinary Center (ESSIC), University of Maryland – College Park,
6 College Park, Maryland, USA

7 ²Department of Meteorology, The Pennsylvania State University, University Park, Pennsylvania,
8 USA

9 ³NASA/Goddard Space Flight Center, Greenbelt, Maryland, USA

10 ⁴Cooperative Institute for Research in Environmental Sciences, University of Colorado, Boulder,
11 Colorado, USA

12 ⁵NOAA Earth System Research Laboratory, Global Monitoring Division, Boulder, Colorado,
13 USA

14 Correspondence to: R. M. Stauffer (ryan.m.stauffer@nasa.gov)

15 **Keywords/Index Terms**

16

17 Tropospheric Ozone – Surface Ozone – Ozonesondes – Self-Organizing Maps – Pollution – STE

18

19 **Key Points**

- 20 • Thin layers of high O₃ 1 – 4 km amsl are frequent over Trinidad Head, CA (TH)
- 21 • STE and pollution transport are difficult to distinguish with observations
- 22 • High TH O₃ coincides with +5 – 10 ppbv surface O₃ at high-elevation monitors

23 **Abstract**

24

25 Much attention has been focused on the transport of ozone (O_3) to the Western U.S.,
26 particularly given the latest revision of the National Ambient Air Quality Standard (NAAQS) to
27 70 parts per billion by volume (ppbv) of O_3 . This makes defining a “background” O_3 amount
28 essential so that the effects of stratosphere-to-troposphere exchange and pollution transport to
29 this region can be quantified. To evaluate free-tropospheric and surface O_3 in the Western U.S.,
30 we use self-organizing maps to cluster 18 years of ozonesonde profiles (940 samples) from
31 Trinidad Head, CA. Two of nine O_3 mixing ratio profile clusters exhibit thin laminae of high O_3
32 above Trinidad Head. A third, consisting of background (~20 – 40 ppbv) O_3 , occurs in ~10% of
33 profiles. The high O_3 layers are located between 1 and 4 km amsl, and reside above a subsidence
34 inversion associated with a northern location of the semi-permanent Pacific subtropical high.
35 Several ancillary data sets are examined to identify the high O_3 sources (reanalyses, trajectories,
36 remotely-sensed carbon monoxide), but distinguishing chemical and stratospheric influences of
37 the elevated O_3 is difficult. There is marked and long-lasting impact of the elevated tropospheric
38 O_3 on high-altitude surface O_3 monitors at Lassen Volcanic and Yosemite National Parks, and
39 Truckee, CA. Days corresponding to the high O_3 clusters exhibit hourly surface O_3 anomalies of
40 +5 – 10 ppbv compared to a climatology; the anomalies can last up to four days. The profile and
41 surface O_3 links demonstrate the importance of regular ozonesonde profiling at Trinidad Head.

42

43 **1. Introduction**

44

45 **1.1. Free-Tropospheric O_3 Contributions to Surface O_3**

46

47 Contributions to the surface O₃ budget are the result of several natural and anthropogenic
48 processes. Free-tropospheric O₃ increases from stratosphere-to-troposphere exchange (STE;
49 Holton et al., 1995; Lin et al., 2012b; 2015; Langford et al., 2009; 2015), intercontinental
50 pollution transport (Huang et al., 2010; Cooper et al., 2011), lightning (Pickering et al., 1998;
51 Kaynak et al., 2008; Ott et al., 2010), and fires (Jaffe et al., 2004; Zhang et al., 2011; 2014) all
52 modify surface O₃ when mixed into the boundary layer. Because these processes cannot be
53 regulated, quantifying their influence is increasingly important given the recent lowering of the
54 Environmental Protection Agency (EPA) National Ambient Air Quality Standard (NAAQS)
55 from 75 ppbv to 70 ppbv O₃.

56 Quantitatively segregating contributions to surface O₃ from STE, transported pollution,
57 and local emissions remains a challenge, especially from an observational standpoint.
58 Furthermore, recent modeling studies show that STE may contribute to the surface O₃ budget
59 much more than previously thought. Surface O₃ increases from STE can outweigh those from
60 Asian pollution transport by up to a factor of three in the high altitudes of the Western U.S. (Lin
61 et al., 2012a; b; Langford et al., 2015).

62

63 **1.2. Ozonesonde Profile Links to Surface O₃**

64

65 For the purpose of measuring O₃ entering the Continental U.S., ozonesondes have been
66 launched at Trinidad Head, CA, approximately weekly since August 1997. Parrish et al. (2010)
67 show a strong correlation between tropospheric O₃ from Trinidad Head sondes and surface O₃ at
68 regional inland surface monitors. Knowledge of this relationship, however, yields little

69 information about the geophysical and chemical processes behind the observed O₃ profiles that
70 have such a link to the surface. It also has not provided a clear definition of background O₃.

71 Stauffer et al. (2016) employed self-organizing maps (SOM) to cluster O₃ mixing ratio
72 (O₃_{MR}) profiles from Trinidad Head and three other Contiguous United States (CONUS) sites.
73 Their study found that clusters of surface – 12 km O₃_{MR} profiles were closely linked with large-
74 scale meteorology, including tropopause and 500 hPa heights, potential vorticity (PV)
75 anomalies/STE, and were not necessarily associated with a particular seasonality. Given the
76 geophysical significance of O₃_{MR} profile clusters and the ability to distinguish processes such as
77 STE, we will employ the SOM technique to Trinidad Head surface – 6 km amsl O₃_{MR} profiles.
78 This narrowed altitude focus allows closer inspection of low to mid-tropospheric O₃ variability,
79 and largely avoids the effect of tropopause O₃ gradients on the clusters. The Parrish et al. (2010)
80 study used Trinidad Head ozonesonde data from June-July-August (JJA); we will extend our
81 analysis to all months. In addition to examination of the links between the clusters of Trinidad
82 Head O₃_{MR} profiles and surface O₃ data, interpretation of the geophysical and chemical
83 characteristics of the O₃ profile clusters adds significance to our results.

84 Essentially, our methodology in this paper will be to re-examine the SOM at Trinidad
85 Head, focusing on O₃_{MR} from surface – 6 km amsl. The analyses will comprise two major
86 efforts: 1) Infer meteorological and chemical characteristics of the SOM clusters using sonde
87 measurements, reanalysis data, and remotely-sensed carbon monoxide (CO) and O₃
88 measurements. Evaluation of remotely-sensed measurements is contained in the Appendix to
89 this paper. 2) Evaluate the correspondence of SOM nodes to nearby elevated surface O₃
90 monitors. Focus will mainly be on surface O₃ associated with SOM clusters that contain profiles
91 with enhanced tropospheric O₃ values.

92

93 **2. Data Sources and Methods**

94

95 **2.1. Clustering Ozonesonde Data with SOM**

96

97 Ozonesonde and radiosonde profiles for Trinidad Head, CA, were obtained from the
98 NOAA Earth System Research Laboratory Global Monitoring Division data archive
99 (<ftp://ftp.cmdl.noaa.gov/data/ozwv/Ozonesonde/>). The data were averaged into 100 m bins for
100 uniformity and compatibility with the SOM algorithm. Every profile set includes altitude,
101 pressure, dry-bulb and potential temperature, relative humidity and frost point, O₃ partial
102 pressure, and O₃_{MR}. A total of 940 ozonesonde profiles from August 1997 – March 2015 are
103 used in this study.

104 A very brief explanation of the SOM algorithm (Kohonen, 1995) is given here. For a
105 complete discussion on SOM, its applications to O₃ profile data, and sensitivity tests comparing
106 SOM and the similar k-means clustering algorithm, see Stauffer et al. (2016; details in
107 Appendix). In the SOM application to O₃_{MR} data, a 2-D array of initial nodes, which are
108 comparable to cluster centroids, is defined, and the SOM algorithm is applied iteratively. After a
109 number of iterations where the O₃_{MR} data are input into the algorithm, the SOM converges to its
110 solution. The O₃_{MR} profiles are separated into exclusive clusters defined by their respective
111 SOM nodes, which are equal to the mean of each cluster's O₃_{MR} profiles. An advantage of the
112 SOM over other methods is the topographical ordering of clusters in the SOM. Similar
113 nodes/clusters are arranged in adjacent positions in the map as will be seen in Results below.
114 Our prior work (Jensen et al., 2012; Stauffer et al., 2016) demonstrates that SOM provides

115 meaningful geophysical characterization of clustered O₃ data when compared to meteorological
116 data.

117 The 100 m averaged surface – 6 km amsl O₃_{MR} data for all profiles are input into the
118 same batch SOM algorithm as in Stauffer et al. (2016). That is, we use a 3x3 SOM with nine
119 clusters to allow direct comparisons with the surface – 12 km Trinidad Head, CA, clusters
120 analyzed in that earlier study. The 940 O₃_{MR} profiles are separated into nine exclusive clusters
121 based on similarity in shape to one of the nine nodes.

122

123 **2.2. Meteorological Data**

124

125 Reanalysis data from the ERA-Interim (Dee et al., 2011) data set were obtained to aid
126 meteorological interpretation of the ozonesonde profile clusters. Variables of geopotential
127 height, temperature, PV, and cloud fraction were obtained at four pressure levels (250, 500, 700,
128 850 hPa), and variables of temperature (2 m), total cloud cover, and MSLP were obtained for the
129 surface. The data are available for every six hours for the entire globe on approximately a 0.7° x
130 0.7° grid.

131 Hybrid Single Particle Lagrangian Integrated Trajectory (HYSPLIT; Draxler and Hess,
132 1997) 10-day forward and backward trajectories were calculated for every Trinidad Head
133 ozonesonde profile. Kinematic trajectories ending at every km from 1 – 5 km at the time and
134 location of ozonesonde launch were computed using meteorological data from the NCEP/NCAR
135 Reanalysis Project (Kalnay et al., 1996).

136

137 **2.3. Surface O₃ Data**

138

139 To investigate links between tropospheric O₃ at the Trinidad Head ozonesonde site and
140 regional surface O₃, data were obtained from high-elevation sites in CA with sufficient record
141 lengths. Only monitors over 1 km amsl with O₃ data since 1997, the start of the Trinidad Head
142 record, are considered. We require the 1 km elevation in an attempt to avoid effects from
143 localized emissions sources from more populated lower elevation areas. This criterion also
144 narrows our site candidates to those that are closer to the altitude of enhanced tropospheric O₃
145 layers over Trinidad Head. Three surface O₃ monitors in CA meet our constraints: Lassen
146 Volcanic National Park (Lassen), White Cloud Mountain in Truckee, CA (Truckee), and
147 Yosemite National Park – Turtleback Dome (Yosemite). Site metadata are listed in Table 1.
148 The Lassen and Yosemite sites both operate year-round, while Truckee is typically operated
149 from May – October, with a few years containing all months. Surface O₃ data were obtained
150 from the Clean Air Status and Trends Network (CASTNET;
151 <http://java.epa.gov/castnet/clearsession.do>; Lassen and Yosemite), and the EPA Air Quality
152 System (AQS) database (<https://aqs.epa.gov/api>; Truckee).

153

154 **2.4. Atmospheric Infrared Sounder (AIRS) Data**

155

156 The Atmospheric Infrared Sounder (AIRS; Aumann et al., 2003) launched on NASA’s
157 Aqua satellite in May 2002, provides vertically-resolved measurements of temperature,
158 humidity, and a number of trace gas species. Daily level 3, version 6, O₃ and CO data
159 (http://acdsc.sci.gsfc.nasa.gov/opendap/Aqua_AIRS_Level3/AIRX3STD.006/) on a 1° x 1°
160 horizontal grid that covers the globe assist our interpretation of the O₃ profile clusters at Trinidad

161 Head. Level 3 data are a quality-checked version of the level 2 swath products from AIRS,
162 output on standard pressure levels. Only data from the ascending (daytime, equatorial crossing
163 time of 1330 LST) node of the Aqua orbit are used here.

164

165 **3. Results**

166

167 The surface – 6 km amsl monthly-averaged O₃_{MR} climatology from Trinidad Head, CA
168 (August 1997 – March 2015), is shown in Figure 1. In terms of O₃_{MR} averages, Trinidad Head
169 exhibits a smaller seasonal cycle than other CONUS ozonesonde sites (Newchurch et al., 2003;
170 Stauffer et al., 2016). A maximum in free-tropospheric O₃ is observed from April – August,
171 when the combination of transported pollution, STE, and photochemical O₃ production has the
172 greatest impact on the site. Ozone averages ~55 – 60 ppbv from 2 – 4 km in April – August. At
173 the surface, an O₃ minimum is observed in July with a maximum in MAM. Persistent inflow of
174 marine boundary layer air from the Pacific keeps surface O₃ generally ≤ 50 ppbv at Trinidad
175 Head year-round (Oltmans et al., 2008). This contrasts with the other CONUS stations where
176 surface O₃ values, mostly in summer, frequently exceed 60 or 70 ppbv (Stauffer et al., 2016).

177

178 **3.1. SOM Clusters**

179

180 Climatological averages yield general information about a site's typical O₃ variability,
181 but often mask shorter-term events that occur throughout the year. The surface – 6 km amsl 3x3
182 SOM O₃_{MR} profile clusters (Figure 2) reveal a more realistic depiction of the O₃ profile
183 variability over Trinidad Head and simple data visualization. Each node in Figure 2 contains a

184 distinct profile shape, with related clusters holding adjacent positions in the SOM manifold. In
185 contrast, the mean, 20th and 80th percentile O₃ for the whole data set is shown in cyan with each
186 cluster in Figure 2. Nodes 1, 4, and 7 include very low amounts (< 40 ppbv) of lower
187 tropospheric O₃, nodes 2, 5, and 8 contain near average (~50 ppbv) O₃ amounts in the low to
188 mid-troposphere, and nodes 3, 6, and 9 contain high (> 60 ppbv) O₃ amounts in layers at
189 progressively higher altitudes.

190 The disparity between the monthly-averaged O₃_{MR} profiles (Figure 1) and the profile
191 nodes (Figure 2) illustrates how much information is lost using simple ozonesonde averages at
192 Trinidad Head. Monthly-averaged O₃_{MR} below 4 km peaks at 62 ppbv in May at Trinidad Head.
193 However, average O₃ in three of the nodes (3, 6, and 9) all exceed this value at some point below
194 4 km, with node 6 exhibiting a maximum of 76 ppbv at 3.2 km amsl, and several profiles with >
195 100 ppbv O₃_{MR}. Nodes 3, 6, and 9 encompass a significant percentage, 26%, of total Trinidad
196 Head profiles, with cluster-average O₃ amounts far exceeding that of any monthly average.

197 The remainder of this paper describes geophysical interpretations of the profiles and links
198 to surface O₃ at the monitoring sites for the SOM nodes. All nine SOM nodes are examined, but
199 our main focus is on nodes 3 and 6, which contain locally high amounts of O₃ in the lower
200 troposphere, node 1, which is very clean throughout the troposphere, and nodes 7 and 9, which
201 appear to have stratospheric influence and very high O₃ amounts above 5 km.

202

203 **3.2. Seasonality and Meteorological Analyses**

204

205 The seasonality of O₃ profiles (Figure 3) reveals results similar to the Stauffer et al.
206 (2016) finding that O₃_{MR} SOM clusters often do not correspond to distinct seasons. Nodes 1, 2,

207 4, and 5 favor certain months, but every month of the year is represented in these clusters. Other
208 nodes contain sharper peaks in the distribution of months. Nodes 3 and 6, which contain high O₃
209 amounts, generally occur in spring and summer. Newchurch et al. (2003) noted that STE events
210 and intrusions of high O₃ into the troposphere were much more frequent at Trinidad Head
211 compared to other CONUS sites, especially in the summer. This may explain the seasonality of
212 profiles in nodes 7 and 9, which are most common between April and August. The cleaner
213 nodes 1 and 4 are analogous to node 7 in Stauffer et al. (2016). Profiles in those clusters are
214 likely affected by subtropical air, and represent baseline/background O₃ amounts over Trinidad
215 Head that are observed during several months of the year.

216 To remove the effects that different seasons may have on meteorological analyses, results
217 here are presented in terms of both SOM node means and anomalies from climatology (1981 –
218 2010 base period). The ERA-Interim 500 hPa height means and anomalies corresponding to
219 each SOM cluster are shown in Figure 4, revealing typical large-scale mid-tropospheric patterns.
220 The polluted nodes 3 and 6 are under, or just downstream of a synoptic-scale ridge, where one
221 would expect subsidence. The large-scale pattern corresponding to node 2 is nearly identical to
222 nodes 3 and 6. However, node 2 seasonality (Figure 3) is essentially the opposite of nodes 3 and
223 6, explaining the O₃ differences among those nodes found in the lower troposphere in Figure 2.
224 Nodes 7 and 9, hypothesized to be impacted by STE, are associated with influence from a trough
225 centered directly over the site. In Stauffer et al. (2016), we showed a strong correlation between
226 500 hPa troughs and O₃ enhancement from STE events. The baseline nodes 1 and 4 exhibit a
227 dichotomy in 500 hPa anomaly patterns, indicating that background tropospheric O₃ mixing
228 ratios can occur under a variety of synoptic conditions at Trinidad Head.

229 The ERA-Interim MSLP means and anomalies (Figure 5) show the influence the position
230 of the semi-permanent Pacific subtropical high has on the Trinidad Head O₃ profiles. Clusters 2,
231 3, and 6 all show MSLP anomalies of +1 – 3 hPa extending into the Pacific Northwest of North
232 America. This is a stark contrast to the MSLP fields corresponding to clusters 1 and 7. Except
233 for cluster 9 (34.7° N), cluster 6 (34.1° N) is the farthest north position of the center ('H' on
234 Figure 5) of the Pacific subtropical high of all the SOM nodes, with other nodes (2, 4, 5, 7)
235 centered 1.5 – 2° latitude farther south. The 500 hPa and MSLP patterns for node 6 are similar
236 to conditions associated with O₃ maxima described during past campaign studies (e.g. Kloesel et
237 al., 1992; Huang et al., 2010; Cai et al., 2016) along the CA coastline and at inland surface sites.
238 Specifically, the CA coast is situated downstream of a 500 hPa ridge, upstream or along a 500
239 hPa trough axis, and influenced by an anomalously positioned Pacific subtropical high that
240 extends higher surface pressures into the Pacific Northwest. The relationship between
241 subsidence presumed from ERA-Interim analyses and high O₃_{MRs} over Trinidad Head warrants
242 further investigation.

243 A side-by-side comparison of SOM node average O₃_{MR}, relative humidity (RH), and
244 potential temperature (θ) in Figure 6 shows clear signs of subsidence influencing the high O₃
245 profiles in nodes 3 and 6. Nodes 3 and 6 exhibit inflection points in the θ profiles and are 3 – 10
246 °C warmer at 1 km amsl than all other clusters. The subsidence interpretation is further
247 supported by cluster 3 and 6 RH that averages > 10% lower than all other clusters in the 2 – 4 km
248 layer. A decrease in RH is expected if water vapor is conserved in a subsiding, warming air
249 parcel. The layers of high O₃ reside above the strong inversion layer at 1 km, evidence that the
250 enhanced O₃ values were transported with the air masses from higher altitudes. Figure 6 also
251 displays a prominent anti-correlation between O₃ and RH.

252 The contoured maps of backward and forward trajectories from HYSPLIT (Figure 7a, b)
253 give a general sense of the transport pathway for each of the SOM clusters. The backward
254 (forward) trajectories end (start) at 3 km amsl, near the altitude of the O₃_{MR} maxima in clusters 3
255 and 6. Though most of the back trajectories are zonal, anti-cyclonic curvature can be visualized,
256 especially in cluster 3. The trajectories also have a more northerly approach along the CA coast
257 in clusters 3 and 6, associated with the mid-tropospheric ridge and the Pacific subtropical high
258 influence extending farther northeast (Figures 4 and 5). Most of the trajectories approach
259 Trinidad Head from higher altitudes, much like those computed in Oltmans et al. (2008).
260 Forward trajectories show a tendency for transport to continue in a meridional direction from
261 Trinidad Head in many clusters, but zonal directions are dominant. The HYSPLIT trajectories
262 did not indicate STE or potential pollution transport from specific regions corresponding to
263 observed high O₃ in clusters 3 and 6.

264 The meteorological evidence presented clearly shows that large-scale synoptic influence
265 and associated subsidence affect the Trinidad Head O₃ profiles. However, distinguishing STE
266 and pollution transport contributions to O₃ in the lower troposphere over Trinidad Head remains
267 difficult with available reanalyses and observations, particularly with this large data set.
268 Analyses of remotely-sensed data from AIRS and a description of our effort to separate pollution
269 transport and STE are presented in the Appendix. In general, analyses of stratospheric (PV) and
270 pollution (CO) indicators yielded mixed and unconvincing results on influences on the profiles.

271

272 **3.3. SOM Links to Surface O₃ Data**

273

274 The monthly-averaged diurnal surface O₃_{MR} over the 18 year record for the three CA
275 surface sites is shown in Figure 8. Lassen is the cleanest site by a large margin, with a maximum
276 in hourly O₃_{MR} of 57 ppbv in July and August. Truckee maximizes at 65 ppbv in July, and
277 Yosemite is, on average, the most polluted, with an hourly maximum of 68 ppbv in both July and
278 August. Lassen and Yosemite both show some influence presumably from regional NO_x
279 emissions sources. This is manifest as a larger diurnal range in O₃_{MR} from NO_x titration at night.
280 More removed from regional influences, Truckee exhibits a minimal diurnal range. As with the
281 Trinidad Head ozonesonde profiles, we find that surface O₃ variability at the three monitoring
282 sites is best understood through links to the Trinidad Head SOM clusters, rather than with simple
283 climatology, because SOM also discriminates subtle but important differences among the three
284 surface sites.

285

286 **3.3.1. Sonde/Surface O₃ Correspondence**

287

288 The relationship between the O₃_{MR} measured by the Trinidad Head ozonesondes and
289 O₃_{MR} at the three surface sites is shown in Figures 9 – 11. At each site, average diurnal O₃_{MR}
290 was calculated for days corresponding to each SOM node (black lines), with the average O₃_{MR}
291 from the sonde plotted in black dots. The sonde O₃_{MR} presented in Figures 9 – 11 is from the
292 same altitude as each respective surface monitor.

293 As in Parrish et al. (2010), our results show that Trinidad Head ozonesondes are
294 representative of regional O₃ levels. There is generally strong agreement (on average ±5 ppbv)
295 between O₃_{MR} from Trinidad Head sondes and the surface monitors for most SOM clusters,
296 particularly at Truckee (Figure 10) and Yosemite (Figure 11). The Lassen site (Figure 9) is

297 cleaner, with average surface O₃_{MR} that is consistently below that measured at Trinidad Head,
298 and rarely exceeds the Trinidad Head value during peak O₃ later in the afternoon. Two
299 exceptions to the agreement between sonde and surface are found in nodes 1 and 7 at all sites.
300 These two clusters at Trinidad Head contain profiles with very low O₃_{MR} in the low to mid-
301 troposphere, but often occur in the summer months. This outcome is similar to that found in
302 Brodin et al. (2011) and Oltmans et al. (1996) – that agreement between ozonesonde and surface
303 data is seasonally dependent. Generally the best agreement occurs when O₃ is low in the winter,
304 and worst in the summer when local photochemistry often causes differences between the
305 surface and free troposphere.

306 SOM nodes 3 and 6, the two polluted Trinidad Head sonde clusters, are associated with
307 the highest surface O₃ at all three monitoring sites. Node 3 and 6 average surface O₃_{MRs} are quite
308 similar to the maximum monthly averages from Figure 8. Lassen node 3 and 6 O₃_{MR} maxima are
309 59 and 60 ppbv, compared to the 57 ppbv maximum in July and August. Truckee node 3 and 6
310 O₃_{MR} maxima are 70 and 68 ppbv, compared to 65 ppbv (July). Yosemite node 3 and 6 O₃_{MR}
311 maxima are 69 and 67 ppbv, compared to 68 ppbv (July and August). However, these results are
312 somewhat misleading because cluster 3 and 6 ozonesondes are not exclusive to the summer
313 months when photochemical O₃ production is highest. Therefore, we choose to calculate surface
314 O₃ anomalies from monthly averages to better assess the impact of the increased tropospheric O₃
315 in nodes 3 and 6.

316 Each day of surface O₃_{MRs} corresponding to a SOM node is compared to its respective
317 monthly climatological O₃_{MR} (measurement – climatology), and the results are averaged for each
318 SOM node. The results of these calculations are shown in Figure 12. In addition to surface
319 measurements for the same day as the Trinidad Head sondes, measurements for one, two, and

320 three days after the sonde date are illustrated to estimate how long O₃ anomalies persist. Ozone
321 anomalies are 5 – 10 ppbv above monthly climatology the same day as the ozonesondes in
322 clusters 3 and 6 at all three sites. In the afternoon and evening hours, Truckee surface O₃_{MR}
323 anomalies peak at +12 ppbv the same day as node 3 profiles. Conversely, surface O₃_{MR}
324 associated with node 7 falls well below (-5 to -10 ppbv) climatology. The synoptic-scale
325 meteorology associated with node 7 is hostile to surface O₃ production.

326 Significant positive O₃_{MR} anomalies of +5 ppbv associated with node 3 and 6 profiles at
327 Trinidad Head linger up to three days after the ozonesonde launch date. Considering that the
328 Yosemite site is 515 km SE of Trinidad Head, this suggests that the Trinidad Head ozonesondes
329 can predict surface O₃ conditions up to four days for an extensive area of CA.

330

331 **3.3.2. Potential Implications for NAAQS**

332

333 The large positive anomalies in surface O₃ at these sites associated with Trinidad Head
334 sondes have significant implications for compliance with the 8-hr NAAQS standard of 70 ppbv.
335 The U.S. NAAQS for 8-hr surface O₃ was revised in October 2015 from the previous value of 75
336 ppbv, to 70 ppbv. The California Air Resources Board (CARB) already approved a statewide 70
337 ppbv O₃ standard equal to the current NAAQS in April 2005. Compliance with the NAAQS, set
338 by the Environmental Protection Agency (EPA), is determined by a region's "design value."
339 The design value is calculated as the three-year running average of the fourth highest maximum
340 daily 8-hr average O₃ (MDA8). Because of the implications for environmental regulation, we
341 evaluate the link between Trinidad Head SOM nodes and MDA8/NAAQS at the surface O₃ sites.

342 The frequency and total number of exceedances of the current NAAQS/CARB O₃
343 standard (70 ppbv) for each Trinidad Head SOM node for the three surface O₃ sites is shown in
344 Table 2. Given the possibility of future, stricter standards, results for a hypothetical 60 ppbv
345 standard are also presented. Results for the surface sites correspond to the same day as the
346 ozonesonde launches. Not surprisingly, the frequency of exceedances corresponding to polluted
347 ozonesonde profiles in clusters 3 and 6 are much higher than the other nodes, maximizing at
348 nearly a 50% frequency at Truckee (70 ppbv standard) on node 3 profile days. Almost 2/3 of
349 node 7 profiles at Trinidad Head are from JJA. However, the exceedance frequency in node 7 at
350 Truckee and Yosemite is half that of the polluted nodes 3 and 6, and there has *never* been a 70
351 ppbv exceedance at Lassen on the day a node 7 profile was observed. Extending this analysis to
352 a stricter 60 ppbv standard shows a dramatic jump in exceedance rates. Under a 60 ppbv
353 standard, the cleaner Lassen site exhibits exceedance rates similar to that of Truckee and
354 Yosemite for the 70 ppbv standard, and there are no 0% exceedance nodes. The two polluted
355 sites both display four SOM nodes containing $\geq 50\%$ exceedance frequency for a 60 ppbv
356 standard. The links between free-tropospheric and surface O₃ must be considered for NAAQS
357 policy discussions as air quality regulations become ever more stringent.

358

359 **4. Summary/Conclusions**

360

361 We performed SOM clustering analysis on the lower tropospheric segment (surface – 6
362 km amsl) of the Trinidad Head ozonesonde dataset, consisting of 940 profiles from 1997 – 2015.
363 As with our prior study of Trinidad Head ozone profiles from the surface to 12 km, we found
364 strong connections between overall O₃ structure and certain meteorological conditions. We also

365 found that most SOM nodes included profiles from a range of seasons. Specifically, polluted O₃
366 profile clusters at Trinidad Head occur when the site is situated in a downstream position from a
367 500 hPa ridge, and subsiding air in an anti-cyclonic pathway around the semi-permanent Pacific
368 subtropical high. These conditions lead to the highest surface O₃ values at three elevated air
369 quality monitoring sites (Lassen, Truckee, and Yosemite) downwind of Trinidad Head; this
370 relationship holds for several days after the sounding is made. The clear links among
371 ozonesonde clusters, diurnal surface O₃, and MDA8/exceedance frequency at these locations
372 have strong implications for the effectiveness of emissions controls and future policy
373 considerations. For example, with a 60 ppbv MDA8 O₃ standard, several polluted ozonesonde
374 SOM nodes are associated with an exceedance on more than half of days at Truckee and
375 Yosemite.

376 The SOM allows identification of baseline O₃ amounts and their associated
377 meteorological conditions, as it does not rely on the simple averaging that generates
378 climatological O₃ values. Background O₃ of ~20-40 ppbv in cluster 1 occurred throughout the
379 year when Trinidad Head was situated between a 500 hPa trough and ridge, and was likely
380 influenced by a subtropical air mass. With the elevated O₃, nominally polluted in a few nodes,
381 the SOM cannot distinguish imported O₃ from long-range transport or STE (see Appendix).
382 However, it is safe to conclude that cases where high tropospheric O₃ is caused exclusively by
383 one process or the other are rare. Profiles will need to be evaluated in conjunction with chemical
384 model output on a case-by-case basis to determine dominant signals affecting the O₃ profile.

385

386 **Appendix A**

387

388 We describe efforts to combine analysis of the Trinidad Head SOM ozonesonde record
389 with remotely-sensed CO and O₃ measurements from AIRS to distinguish STE and transported
390 pollution contributions to O₃ profiles over the 14.5 year record. Stratospheric intrusions of air
391 deep into the troposphere typically contain low amounts of CO and water vapor, and high
392 amounts of O₃ and PV (Browell et al., 1996; Ott et al., 2016). Layers of transported pollution
393 generally contain higher CO compared to typical tropospheric concentrations in conjunction with
394 high O₃. Lin et al. (2012a) were able to use AIRS CO to detect influence from Asian emissions
395 during the CalNex campaign in May – June 2010.

396 Data from AIRS was analyzed at 700 hPa (~3 km amsl, near the altitude of maximum O₃)
397 in nodes 3 and 6) to identify potential pollution signatures in the Trinidad Head profiles. The
398 same SOM output from the body of this paper is used, truncated to the AIRS data record length
399 (September 2002 – March 2015). There is a distinct seasonal cycle of CO, so we present results
400 in terms of anomalies from monthly means from the AIRS record.

401 The SOM node-averaged CO anomalies (Figure A1) provide compelling evidence for
402 only a few of the Trinidad Head O₃ clusters. For example, node 1 exhibits an average CO
403 anomaly of -4 ppbv. This is characteristic of clean, subtropical air influencing Trinidad Head
404 given the low O₃_{MRs} throughout the surface – 6 km profile in node 1. The highest CO anomalies
405 occur in node 6, averaging 5 ppbv above climatology, indicating frequent pollution events on
406 those days. The Trinidad Head site lies directly between a dipole of negative and positive CO
407 anomalies in node 3, so we examine the individual cases to determine if separating influence
408 from pollution and STE in the O₃ profiles is possible.

409 Figure A2 shows an analysis of CO, PV, and O₃_{MR} at 700 hPa over the Trinidad Head
410 site. Nodes 3 and 6, which contain the highest O₃_{MRs} at this level, are distinguished from the

411 other nodes on the plot. One might expect an inverse relationship between PV and CO, but no
412 such relationship is evident in Figure A2. There are individual cases that suggest low CO/high
413 PV STE cases and vice versa, but there are also exceptions. Using RH and CO as a proxy for
414 STE (not shown) also yields inconclusive results. Thus, the low altitudes where we observe high
415 O₃ over Trinidad Head may be too far removed from both pollution and STE sources to separate
416 them.

417 The SOM node-averaged O₃ anomalies (Figure A3) display the inability of AIRS to
418 detect the thin layers of high O₃ observed in nodes 3 and 6 at Trinidad Head. In fact, AIRS
419 reports *negative* O₃_{MR} anomalies at 700 hPa in nodes 3 and 6. The true O₃_{MR} anomalies as
420 measured by the ozonesondes average between 8 – 15 ppbv above the monthly climatology. The
421 O₃ distributions in Figure A3 appear to be tuned toward O₃_{MRs} found at higher altitudes near 5 –
422 6 km amsl (see Figure 2). Nodes 1, 7, and 9, which all have notably high or low O₃_{MR} at 5 – 6
423 km, also display large AIRS O₃ anomalies. This effect likely arises because of the vertical
424 sensitivity of the AIRS instrument. AIRS is most sensitive in the mid-troposphere, generally
425 between 300 – 600 hPa (Warner et al., 2007; Thonat et al., 2012). Thus, the majority of
426 information input into the retrieval algorithm comes from above the O₃ maxima found in SOM
427 nodes 3 and 6. The fact that the thin layers of high O₃ above Trinidad Head are unnoticed by
428 AIRS shows that the satellite is no substitute for ozonesonde profiling.

429 The likelihood that many profiles contain elements of both STE and pollution make
430 definitive characterization of the SOM nodes difficult. Additional information from chemical
431 transport model output will be analyzed in future studies to determine the frequency and
432 magnitude of STE and pollution effects on the Trinidad Head ozonesonde profiles.

433

434 **Acknowledgments**

435

436 Funding for this project was provided by the following NASA grants: NNG05G062G,
437 NNX10AR39G, NNX11AQ44G, and NNX12AF05G. This paper is the basis for a chapter in the
438 first author's PhD dissertation. NOAA ESRL GMD data (Trinidad Head ozonesondes) accessed
439 at: <ftp://ftp.cmdl.noaa.gov/data/ozwv/Ozonesonde/>. ERA-Interim reanalysis data accessed at:
440 <http://rda.ucar.edu/datasets/ds627.0/>. NCEP/NCAR reanalysis data accessed at:
441 <ftp://ftp.cdc.noaa.gov/>. AIRS CO and O₃ data accessed at:
442 http://acdsc.sci.gsfc.nasa.gov/opendap/Aqua_AIRS_Level3/AIRX3STD.006/. Surface O₃ data
443 accessed at: <http://java.epa.gov/castnet/clearsession.do> (Lassen and Yosemite), and
444 <https://aqs.epa.gov/api> (Truckee). Thanks to Professors Dr. George Young and Dr. William
445 Brune (Penn State) for valuable comments and suggestions for meteorological analyses.

446

447 References

448

- 449 Aumann, H. H., M. T. Chahine, C. Gautier, M. Goldberg, E. Kalnay, L. McMillin, H.
450 Revercomb, P. W. Rosenkranz, W. L. Smith, D. Staelin, L. Strow, and J. Susskind
451 (2003), AIRS/AMSU/HSB on the Aqua mission: Design, science objectives, data
452 products and processing systems, *IEEE T. Geosci. Remote*, 41, 253–264,
453 doi:10.1109/TGRS.2002.808356.

454 Brodin, M., D. Helmig, B. J. Johnson, and S. J. Oltmans (2011), Comparison of ozone
455 concentrations on a surface elevation gradient with balloon-borne ozonesonde
456 measurements, *Atmos. Environ.*, 45, 5431-5439, doi:10.1016/j.atmosenv.2011.07.002.

457 Browell, E. V., et al. (1996), Large-scale air mass characteristics observed over western Pacific
458 during summertime, *J. Geophys. Res.*, 101(D1), 1691–1712, doi:10.1029/95JD02200.

459 Cai, C., et al. (2016), Simulating reactive nitrogen, carbon monoxide, and ozone in California
460 during ARCTAS-CARB 2008 with high wildfire activity, *Atmos. Environ.*, 108, 28 – 44,
461 doi:10.1016/j.atmosenv.2015.12.031.

462 Cooper, O. R., et al. (2011), Measurement of western U.S. baseline ozone from the surface to the
463 tropopause and assessment of downwind impact regions, *J. Geophys. Res.*, 116, D00V03,
464 doi:10.1029/2011JD016095.

465 Dee, D. P., et al. (2011), The ERA-Interim reanalysis: Configuration and performance of the data
466 assimilation system, *Q. J. R. Meteorol. Soc.*, 137, 553-597, doi:10.1002/qj.828.

467 Draxler, R. R., and G. D. Hess (1997), Description of the HYSPLIT_4 modeling system, NOAA
468 Tech. Memo, ERL ARL-224, NOAA Air Resources Laboratory, Silver Spring, MD, 24
469 pp.

- 470 Holton, J. R., P. H. Haynes, M. E. McIntyre, A. R. Douglass, R. B. Rood, and L. Pfister (1995),
471 Stratosphere-troposphere exchange, *Rev. Geophys.*, 33(4), 403-439,
472 doi:10.1029/95RG02097.
- 473 Huang, M., et al. (2010), Impacts of transported background ozone on California air quality
474 during the ARCTAS-CARB period – a multi-scale modeling study, *Atmos. Chem. Phys.*,
475 10, 6947-6968, doi:10.5194/acp-10-6947-2010.
- 476 Jaffe, D., I. Bertschi, L. Jaeglé, P. Novelli, J. S. Reid, H. Tanimoto, R. Vingarzan, and D. L.
477 Westphal (2004), Long-range transport of Siberian biomass burning emissions and
478 impact on surface ozone in western North America, *Geophys. Res. Lett.*, 31, L16106,
479 doi:10.1029/2004GL020093.
- 480 Jensen, A. A., A. M. Thompson, and F. J. Schmidlin (2012), Classification of Ascension Island
481 and Natal ozonesondes using self-organizing maps, *J. Geophys. Res.*, 117, D04302, doi:
482 10.1029/2011JD016573.
- 483 Kalnay, E., et al. (1996), The NCEP/NCAR 40-year reanalysis project, *Bull. Amer. Meteorol.
484 Soc.*, 77, 437–471, doi:[http://dx.doi.org/10.1175/1520-0477\(1996\)077<0437:TNYRP>2.0.CO;2](http://dx.doi.org/10.1175/1520-0477(1996)077<0437:TNYRP>2.0.CO;2).
- 486 Kaynak, B., Y. Hu, R. V. Martin, A. G. Russel, Y. Choi, and Y. Wang (2008), The effect of
487 lightning NO_x production on surface ozone in the continental United States, *Atmos.
488 Chem. Phys.*, 8, 5151-5159, doi:10.5194/acp-8-5151-2008.
- 489 Kloesel, K. A. (1992), Marine stratocumulus cloud clearing episodes observed during FIRE,
490 *Mon. Wea. Rev.*, 120, 565–578, doi:[http://dx.doi.org/10.1175/1520-0493\(1992\)120<0565:MSCCEO>2.0.CO;2](http://dx.doi.org/10.1175/1520-0493(1992)120<0565:MSCCEO>2.0.CO;2).

- 492 Kohonen, T. (1995), The Basic SOM, in Self-Organizing Maps, pp. 77–130, Springer, New
493 York.
- 494 Langford, A. O., K. C. Aikin, C. S. Eubank, and E. J. Williams (2009), Stratospheric
495 contribution to high surface ozone in Colorado during springtime, *Geophys. Res. Lett.*,
496 36, L12801, doi:10.1029/2009GL038367.
- 497 Langford, A. O., et al. (2015), An overview of the 2013 Las Vegas Ozone Study (LVOS): Impact
498 of stratospheric intrusions and long-range transport on surface air quality, *Atmos.*
499 *Environ.*, 109, 305-322, doi:10.1016/j.atmosenv.2014.08.040.
- 500 Lin, M., et al. (2012a), Transport of Asian ozone pollution into surface air over the western
501 United States in spring, *J. Geophys. Res.*, 117, D00V07, doi:10.1029/2011JD016961.
- 502 Lin, M., A. M. Fiore, O. R. Cooper, L. W. Horowitz, A. O. Langford, H. Levy II, B. J. Johnson,
503 V. Naik, S. J. Oltmans, and C. J. Senff (2012b), Springtime high surface ozone events
504 over the western United States: Quantifying the role of stratospheric intrusions, *J.*
505 *Geophys. Res.*, 117, D00V22, doi:10.1029/2012JD018151.
- 506 Lin, M., A. M. Fiore, L. W. Horowitz, A. O. Langford, S. J. Oltmans, D. Tarasick, and H. E.
507 Rieder (2015), Climate variability modulates western U.S. ozone air quality in spring via
508 deep stratospheric intrusions, *Nat. Commun.*, 6, 7105, doi:10.1038/ncomms8105.
- 509 Newchurch, M. J., M. A. Ayoub, S. Oltmans, B. Johnson, and F. J. Schmidlin (2003), Vertical
510 distribution of ozone at four sites in the United States, *J. Geophys. Res.*, 108(D1), 4031,
511 doi:10.1029/2002JD002059.
- 512 Oltmans, S. J., D. J. Hofmann, J. A. Lathrop, J. M. Harris, W. D. Komhyr, and D. Kuniyuki
513 (1996), Tropospheric ozone during Mauna Loa Observatory Photochemistry Experiment

- 514 2 compared to long-term measurements from surface and ozonesonde observations, *J.*
515 *Geophys. Res.*, 101(D9), 14569-14580, doi:10.1029/95JD03004.
- 516 Oltmans, S. J., A. S. Lefohn, J. M. Harris, and D. S. Shadwick (2008), Background ozone levels
517 of air entering the west coast of the US and assessment of longer-term changes, *Atmos.*
518 *Environ.*, 42, 6020-6038, doi:10.1016/j.atmosenv.2008.03.034.
- 519 Ott, L. E., K. E. Pickering, G. L. Stenchikov, D. J. Allen, A. J. DeCaria, B. Ridley, R.-F. Lin, S.
520 Lang, and W.-K. Tao (2010), Production of lightning NO_x and its vertical distribution
521 calculated from three-dimensional cloud-scale chemical transport model simulations, *J.*
522 *Geophys. Res.*, 115, D04301, doi:10.1029/2009JD011880.
- 523 Ott, L. E., B. N. Duncan, A. M. Thompson, G. Diskin, Z. Fasnacht, A. O. Langford, M. Lin, A.
524 M. Molod, J. E. Nielsen, S. E. Pusede, A. J. Weinheimer, and Y. Yoshida (2016),
525 Frequency and impact of summertime stratospheric intrusions over Maryland during
526 DISCOVER-AQ (2011): New evidence from NASA's GEOS-5 simulations, *J. Geophys.*
527 *Res.*, 121, doi:10.1002/2015JD024052.
- 528 Parrish, D. D., K. C. Aikin, S. J. Oltmans, B. J. Johnson, M. Ives, and C. Sweeny (2010),
529 Impacts of transported background ozone inflow on summertime air quality in a
530 California ozone exceedance area, *Atmos. Chem. Phys.*, 10, 10093-10109, doi:
531 10.5194/acp-10-10093-2010.
- 532 Pickering, K. E., Y. Wang, W.-K. Tao, C. Price, and J.-F. Müller (1998), Vertical distributions of
533 lightning NO_x for use in regional and global chemical transport models, *J. Geophys. Res.*,
534 103(D23), 31203–31216, doi:10.1029/98JD02651.

- 535 Stauffer, R. M., A. M. Thompson, and G. S. Young (2016), Tropospheric ozonesonde profiles at
536 long-term U.S. monitoring sites: 1. A climatology based on self-organizing maps, *J.*
537 *Geophys. Res. Atmos.*, 121, 1320-1339, doi:10.1002/2015JD023641.
- 538 Thonat, T., C. Crevoisier, N. A. Scott, A. Chèdin, T. Schuck, R. Armante, and L. Crèpeau
539 (2012), Retrieval of tropospheric CO column from hyperspectral infrared sounders –
540 application to four years of Aqua/AIRS and MetOp-A/IASI, *Atmos. Meas. Tech.*, 5, 2413
541 – 2429, doi:10.5194/amt-5-2413-2012.
- 542 Warner, J., M. M. Comer, C. D. Barnet, W. W. McMillan, W. Wolf, E. Maddy, and G. Sachse
543 (2007), A comparison of satellite tropospheric carbon monoxide measurements from
544 AIRS and MOPITT during INTEX-A, *J. Geophys. Res.*, 112, D12S17,
545 doi:10.1029/2006JD007925.
- 546 Zhang, L., D. J. Jacob, N. V. Downey, D. A. Wood, D. Blewitt, C. C. Carouge, A. van
547 Donkelaar, D. B. A. Jones, L. T. Murray, and Y. Wang (2011), Improved estimate of the
548 policy-relevant background ozone in the United States using the GEOS-Chem global
549 model with 1/2° x 1/3° horizontal resolution over North America, *Atmos. Environ.*, 45,
550 6769-6776, doi:10.1016/j.atmosenv.2011.07.054.
- 551 Zhang, L., D. J. Jacob, X. Yue, N. V. Downey, D. A. Wood, and D. Blewitt (2014), Sources
552 contributing to background surface ozone in the US Intermountain West, *Atmos. Chem.*
553 *Phys.*, 14, 5295-5309, doi:10.5194/acp-14-5295-2014.
- 554
- 555
- 556

557 Table 1: Information on sites used in this study.

558

<u>Monitoring Site</u>	<u>Lat/Lon(°)</u>	<u>Altitude (m)</u>	<u>Dates Used</u>	<u>Distance to Trinidad Head (km)</u>
Trinidad Head	40.8/-124.2	20	1997 – 2015	N/A
Lassen	40.5/-121.6	1756	1997 – 2015	219
Truckee	39.3/-120.8	1335	1997 – Oct. 2014	327
Yosemite	37.7/-119.7	1605	1997 – 2015	515

559

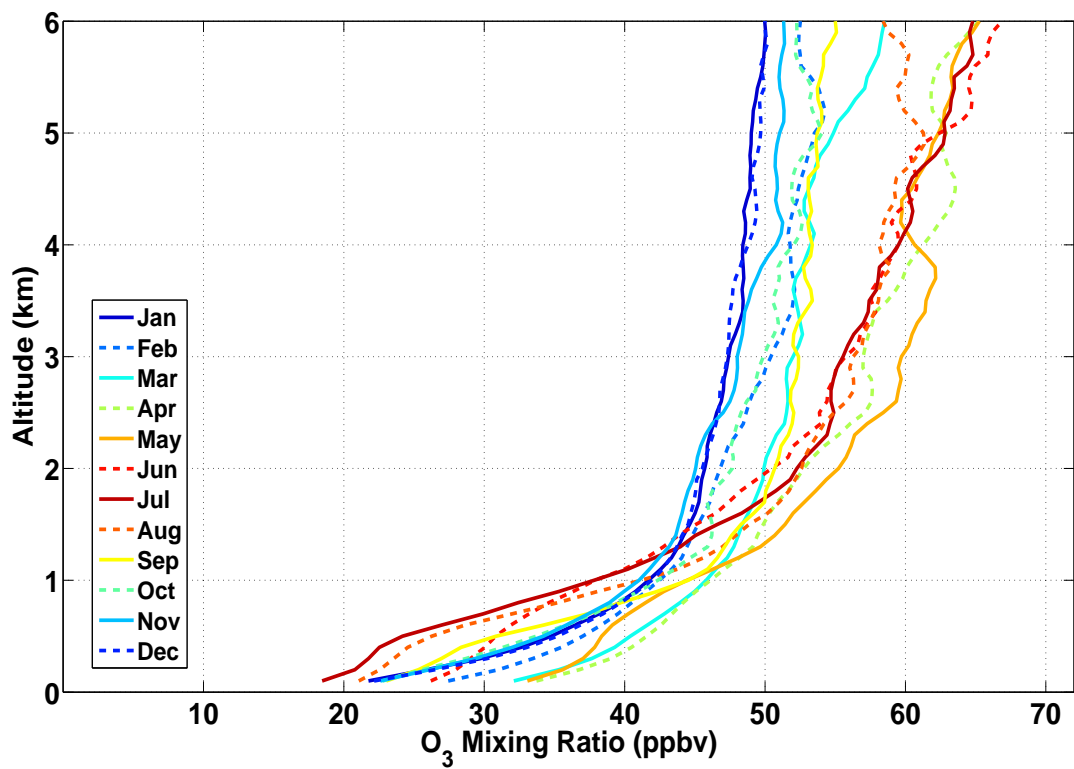
560

561 Table 2: Surface O₃ site frequency of exceeding the 70 ppbv NAAQS/CARB MDA8 surface
 562 O₃_{MR} standard, and a hypothetical 60 ppbv standard, coincident with each SOM node from
 563 Trinidad Head, CA, O₃ profiles. Statistics for the surface sites are for the same day as the
 564 ozonesonde profile. Values $\geq 40\%$ are in bold.

565

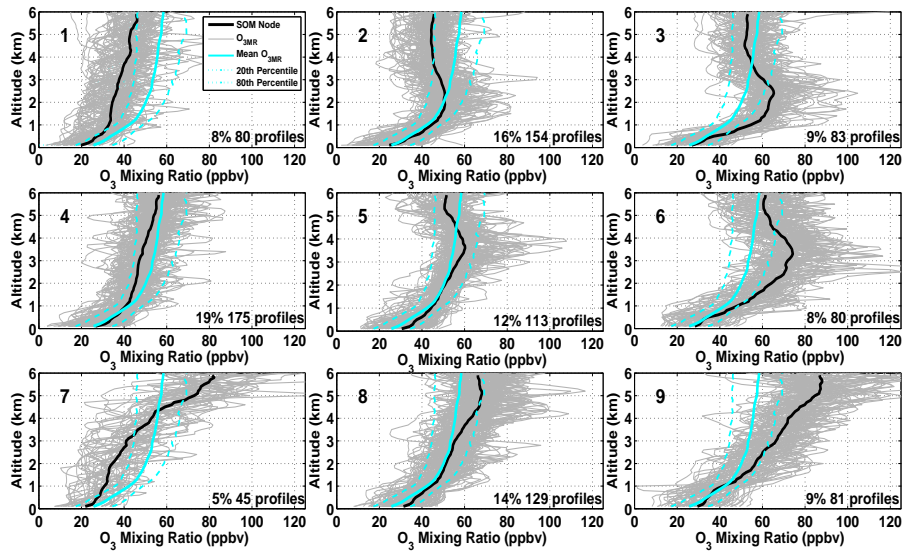
<u>Node</u>	<u>Lassen Volcanic</u>	<u>Truckee</u>	<u>Yosemite</u>
(>70 ppbv)			
1	2.5%, (2 days)	16.4%, (9 days)	21.3%, (17 days)
2	0.6%, (1 day)	31.7%, (20 days)	13.6%, (21 days)
3	12.0%, (10 days)	47.7%, (31 days)	37.3%, (31 days)
4	0.0%, (0 days)	10.0%, (7 days)	5.1%, (9 days)
5	0.9%, (1 day)	14.8%, (8 days)	11.5%, (13 days)
6	12.5%, (10 days)	39.7%, (27 days)	40.0%, (32 days)
7	0.0%, (0 days)	17.9%, (7 days)	17.8%, (8 days)
8	1.6%, (2 days)	9.3%, (7 days)	14.7%, (19 days)
9	6.2%, (5 days)	29.4%, (20 days)	29.6%, (24 days)
(>60 ppbv)			
1	6.3%, (5 days)	34.5%, (19 days)	42.5%, (34 days)
2	7.1%, (11 days)	54.0%, (34 days)	25.3%, (39 days)
3	28.9%, (24 days)	80.0%, (52 days)	61.4%, (51 days)
4	4.0%, (7 days)	25.7%, (18 days)	14.3%, (25 days)
5	4.4%, (5 days)	37.0%, (20 days)	28.3%, (32 days)
6	40.0%, (32 days)	64.7%, (44 days)	62.5%, (50 days)
7	17.8%, (8 days)	33.3%, (13 days)	51.1%, (23 days)
8	12.4%, (16 days)	36.0%, (27 days)	34.9%, (45 days)
9	28.4%, (23 days)	50.0%, (34 days)	56.8%, (46 days)

566



567
568

Figure 1: Monthly-averaged O_3 MR profiles for Trinidad Head, CA, from surface to 6 km amsl.



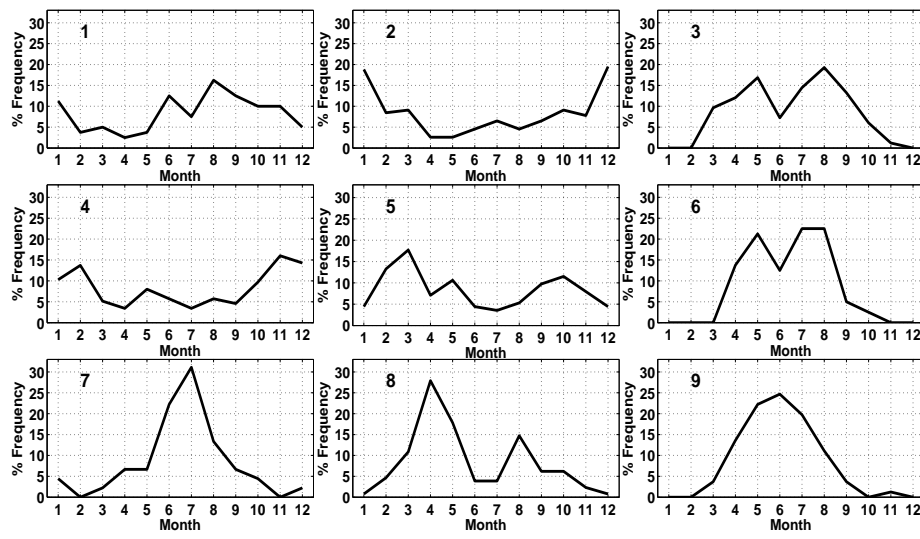
569

570 Figure 2: 3x3 SOM surface – 6 km amsl $O_{3\text{MR}}$ output for Trinidad Head. The SOM nodes
 571 (cluster average O_3) are shown in black, with the individual $O_{3\text{MR}}$ profiles in gray. The overall
 572 mean $O_{3\text{MR}}$ (cyan), 20th and 80th percentile $O_{3\text{MR}}$ (dashed cyan) are shown on all plots. The
 573 percentage of the total profiles and number of profiles in each SOM node appear on the figures.

574

575

576



577

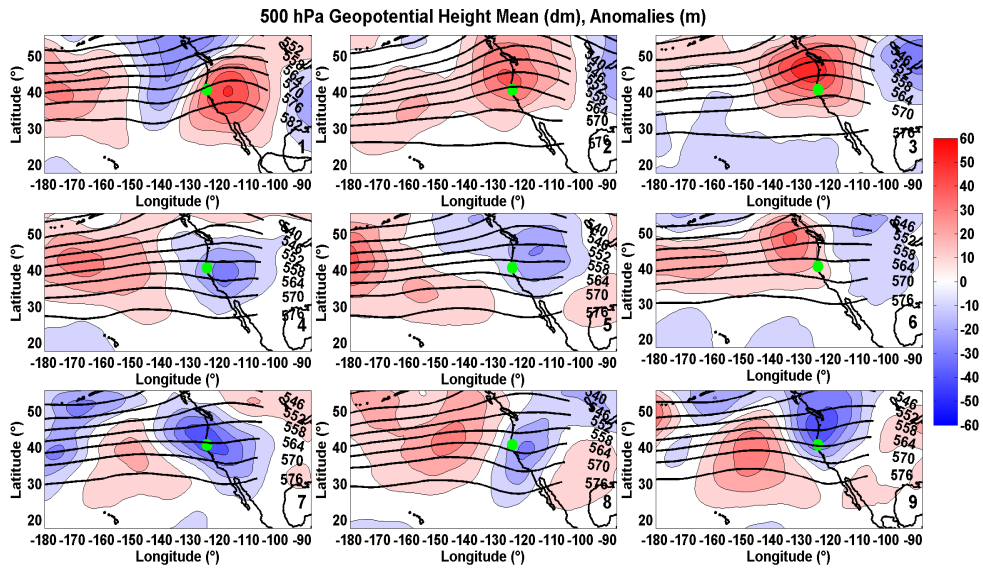
578 Figure 3: Seasonality corresponding to each SOM node from Trinidad Head, shown as the
 579 relative frequency of months within each SOM node. Each histogram totals 100%.

580

581

582

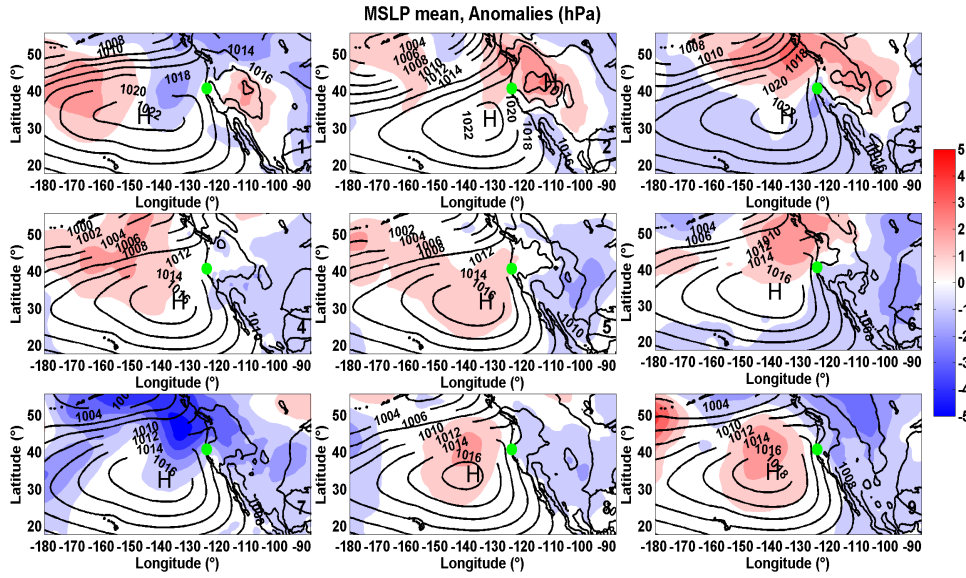
583



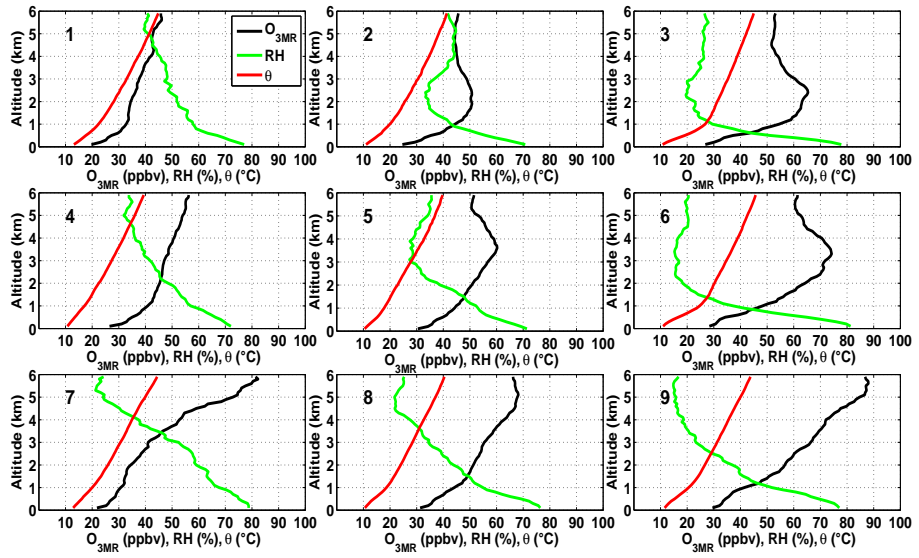
584

585 Figure 4: Contoured map of average ERA-Interim 500 hPa geopotential heights and height
 586 anomalies from climatology corresponding to each SOM node. Anomaly data are contoured
 587 every 10 m from -60 to 60 m. Averaged data are contoured every 6 dm. Blue colors represent
 588 negative anomalies and red colors represent positive anomalies. The green dot represents the
 589 Trinidad Head site location.

590



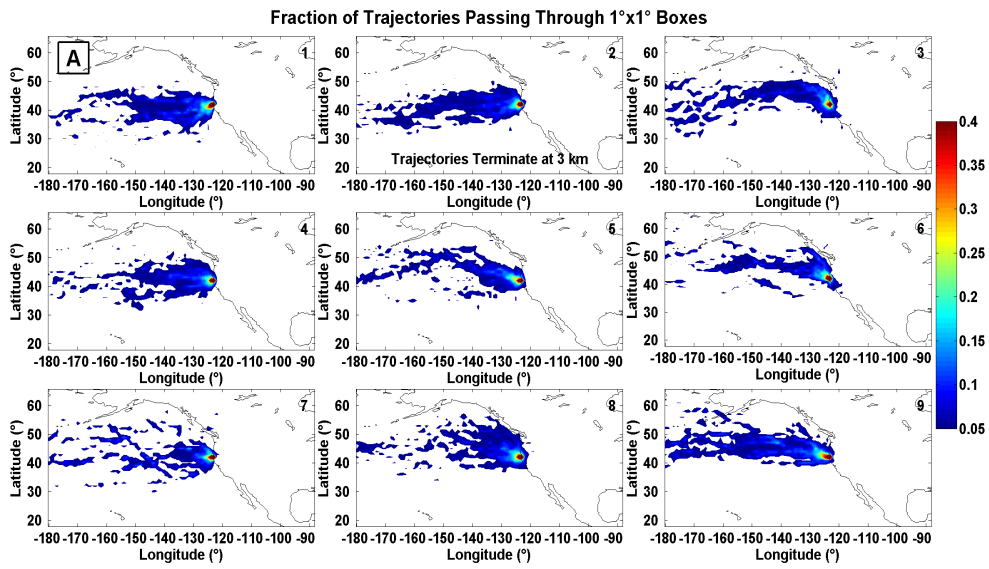
591
592 Figure 5: Contoured map of average ERA-Interim MSLP and MSLP anomalies from
593 climatology corresponding to each SOM node. Anomaly data are contoured every 1 hPa from -5
594 to 5 hPa. Averaged data are contoured every 2 hPa. Blue colors represent negative anomalies
595 and red colors represent positive anomalies. The green dot represents the Trinidad Head site
596 location.
597



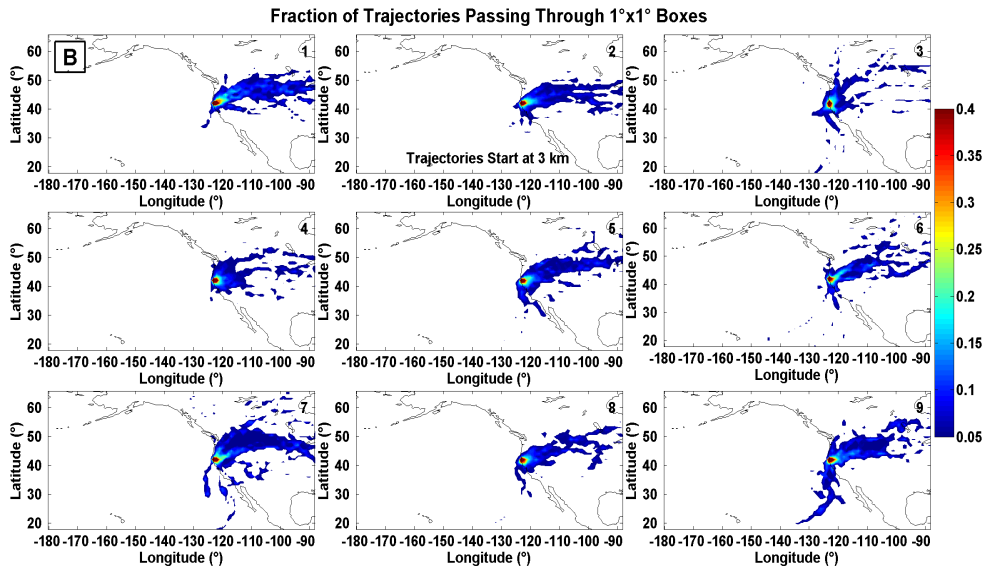
598

599 Figure 6: Profiles of average $O_{3\text{MR}}$ (equivalent to SOM node), RH
600 corresponding to each SOM node at Trinidad Head.

601



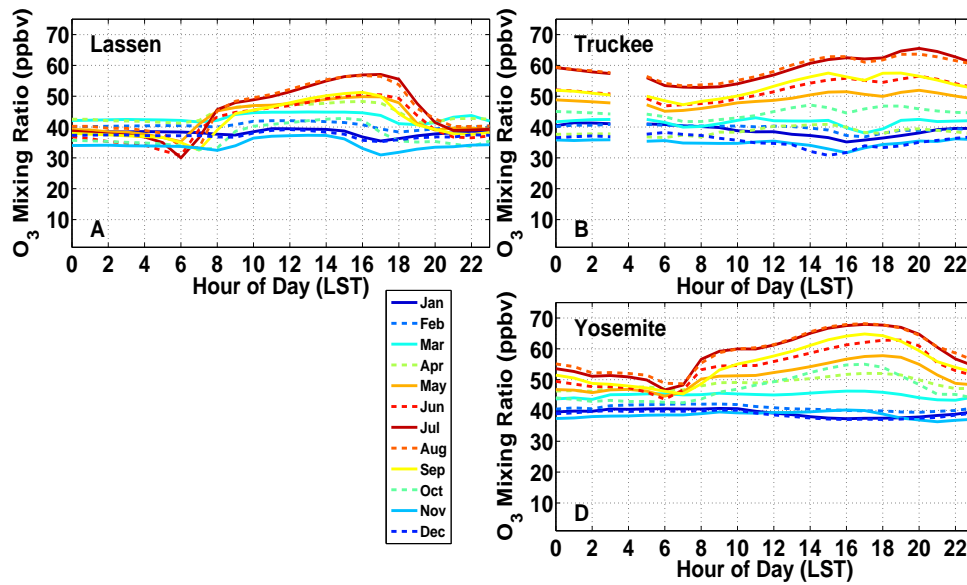
602



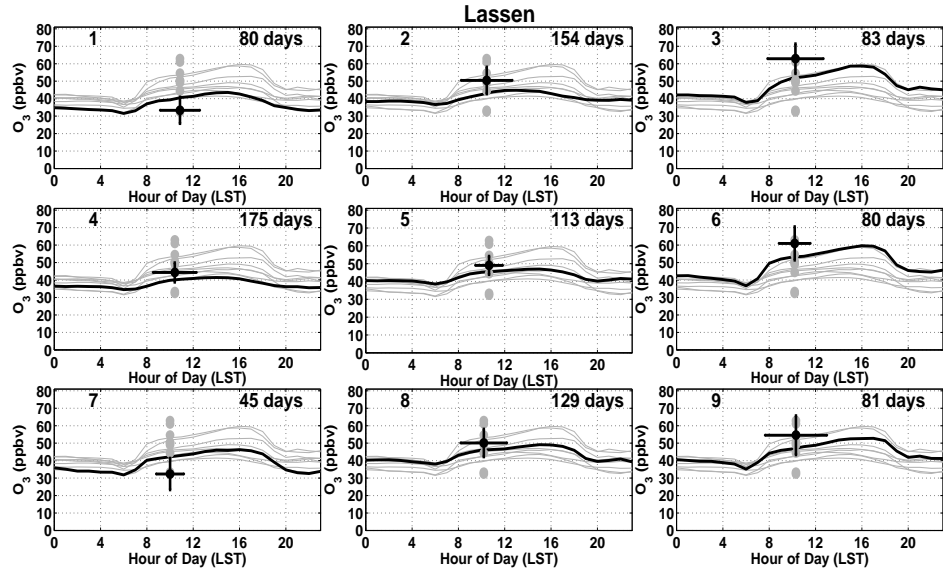
603

604 Figure 7: Contoured maps of HYSPLIT 10-day backward (A, top) and forward (B, bottom)
 605 trajectories terminating/starting at 3 km at time and location of O₃ profiles corresponding to each
 606 SOM node. Data are contoured based on the fraction of trajectories passing through $1^\circ \times 1^\circ$ grid
 607 boxes. Contours are drawn every 0.01 from 0.05 to 0.40.

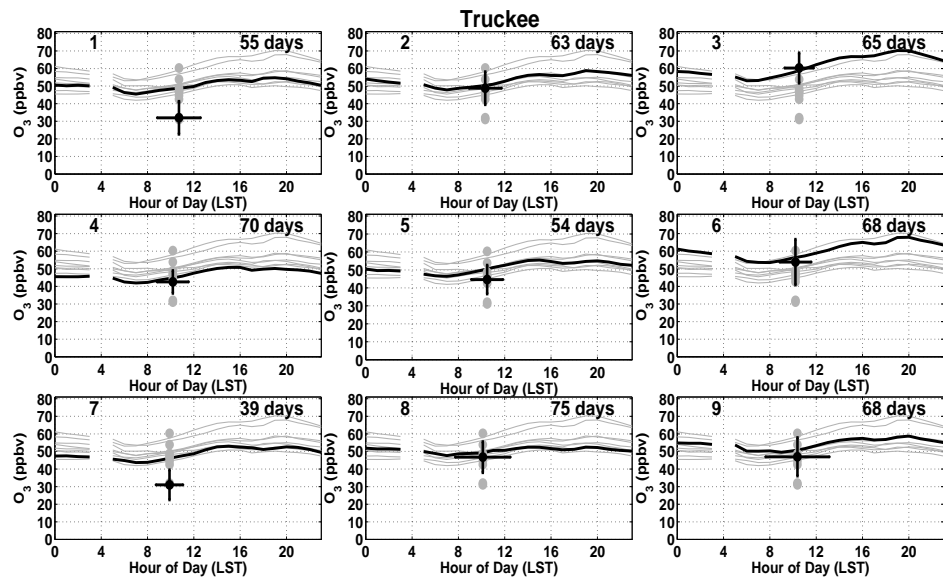
608



609
 610 Figure 8: Monthly-averaged diurnal O_3 MRs for each surface monitoring site. LST hour 04 was
 611 removed from Truckee because of lack of data.



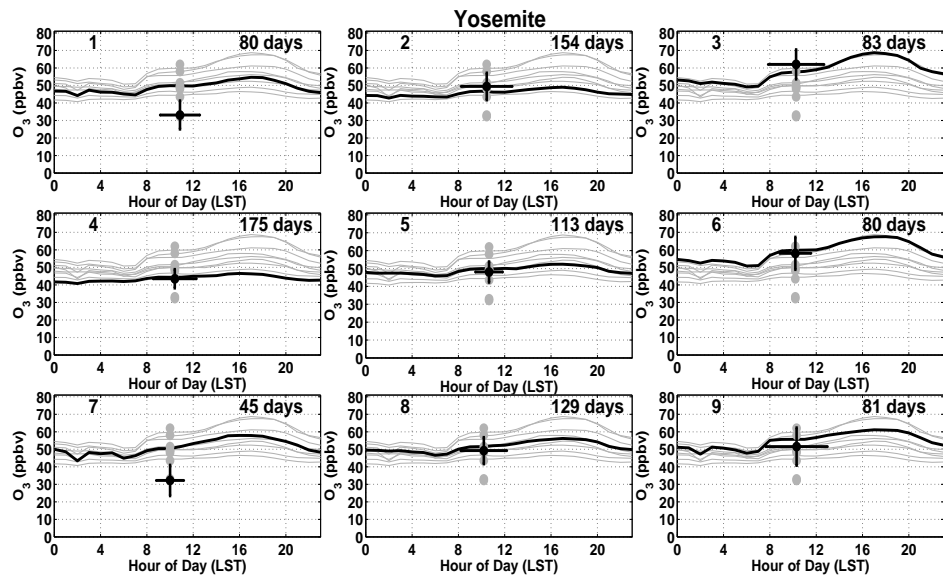
612
 613 Figure 9: Mean diurnal surface O_3 MR at Lassen Volcanic National Park corresponding to each
 614 SOM node. All surface O_3 MR average values are shown, with values corresponding to the SOM
 615 node of interest highlighted by the black line. Black dots represent the SOM node average
 616 ozonesonde O_3 MR corresponding to the same altitude as each surface O_3 site. Lines marking ± 1
 617 standard deviation beyond average ozonesonde O_3 MR and ozonesonde launch time are also
 618 shown. The number of days of surface O_3 data corresponding to each SOM node is shown in
 619 each frame.
 620



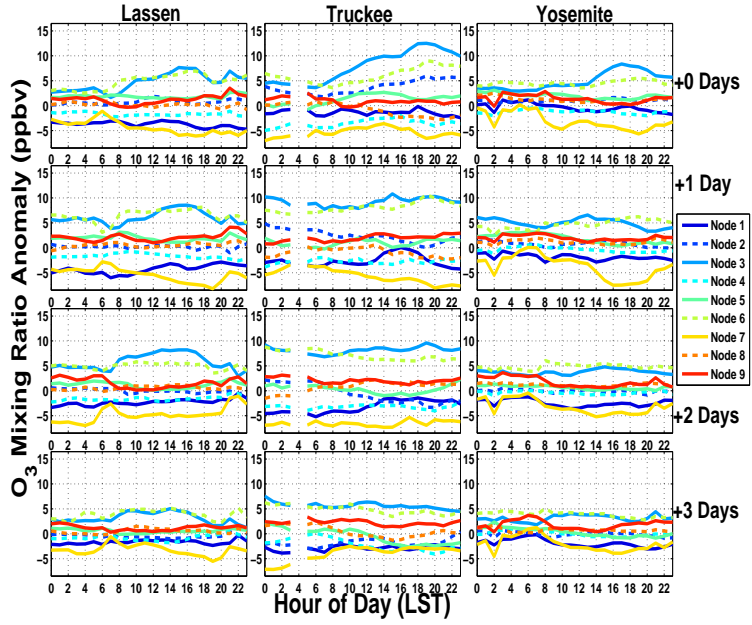
621

622 Figure 10: As in Figure 9, but for the Truckee surface O_3 monitor. LST hour 04 was removed
623 because of lack of data.

624



625
626 Figure 11: As in Figure 9, but for the Yosemite National Park – Turtleback Dome surface O₃
627 monitor.
628

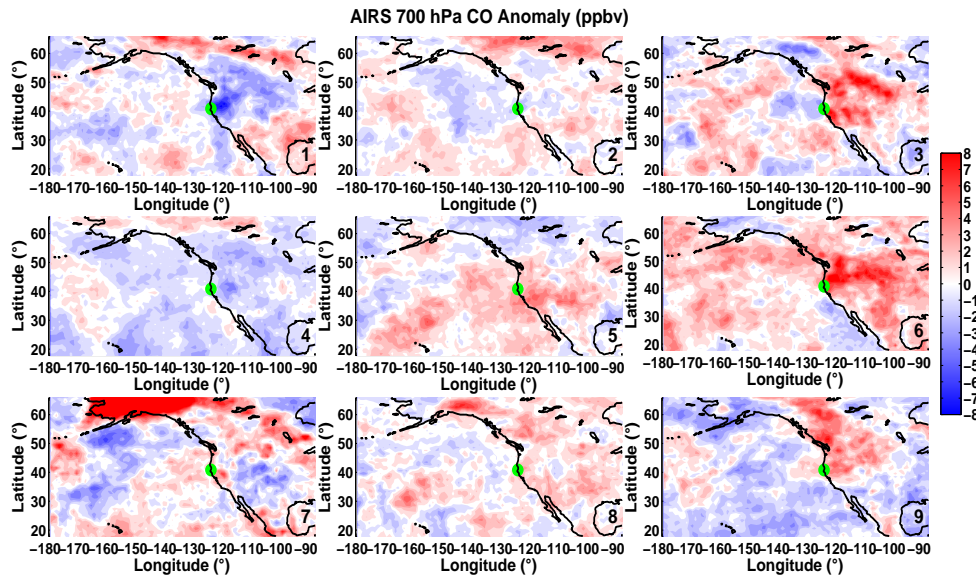


629

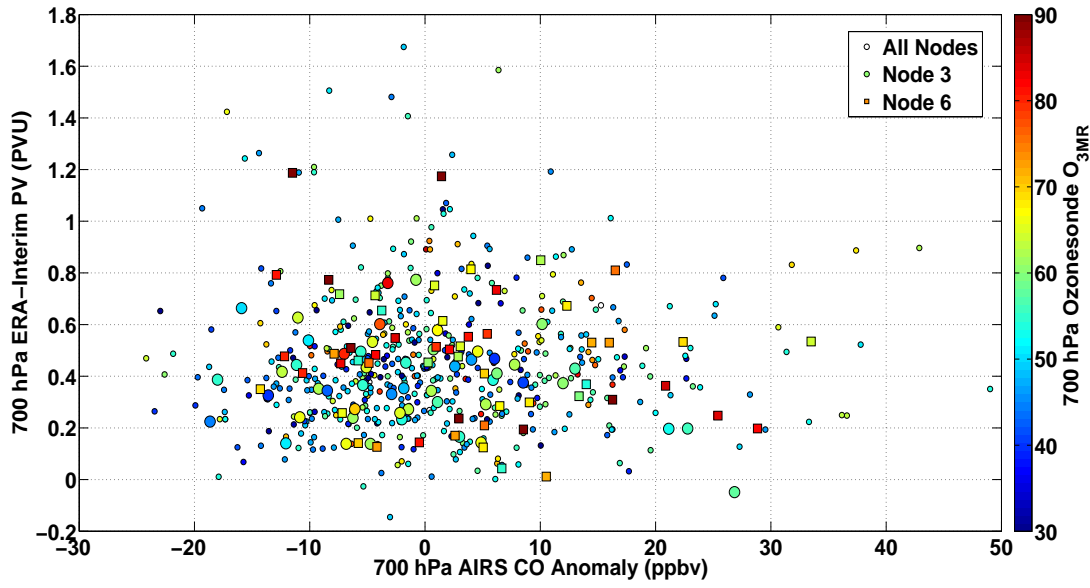
630 Figure 12: Average diurnal surface O₃_{MR} anomalies corresponding to each SOM node. Data
 631 from each site (columns) is given for the same day as the ozonesonde profile, up to three days
 632 after the profile date (rows).

633

634



635
636 Figure A1: Contoured map of average AIRS 700 hPa CO anomalies from monthly climatology
637 corresponding to each SOM node. Data are contoured every 1 ppbv from -8 to 8 ppbv. Blue
638 colors represent negative anomalies and red colors represent positive anomalies. The green dot
639 represents the Trinidad Head site location.
640

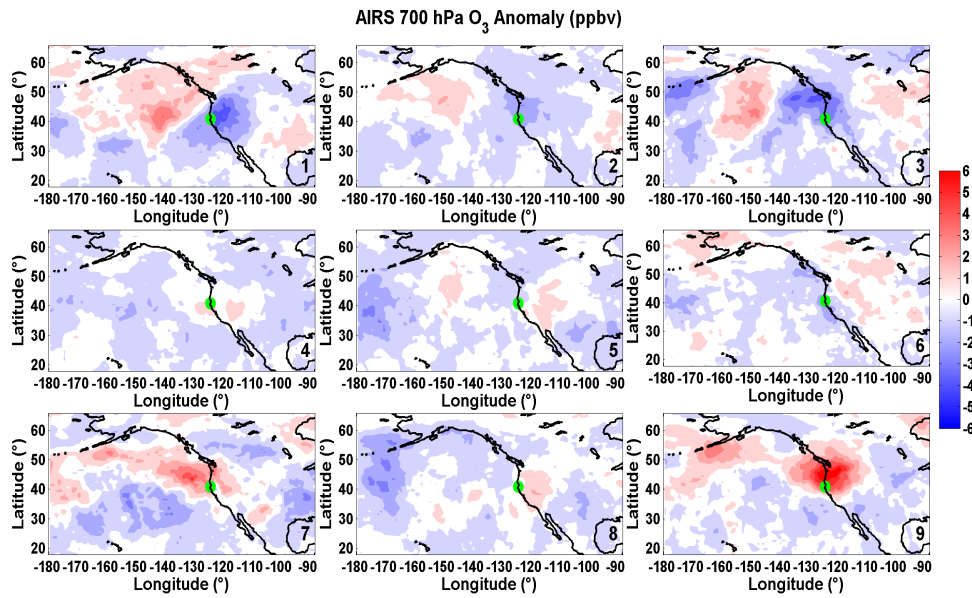


641

642 Figure A2: Scatterplot of 700 hPa AIRS CO anomaly (ppbv) and ERA-Interim PV (PVU), with
 643 700 hPa O₃_{MR} from Trinidad Head ozonesondes in colors. Node 3 points are large circles, node
 644 6 points are large squares, and the remaining nodes' points are small circles.

645

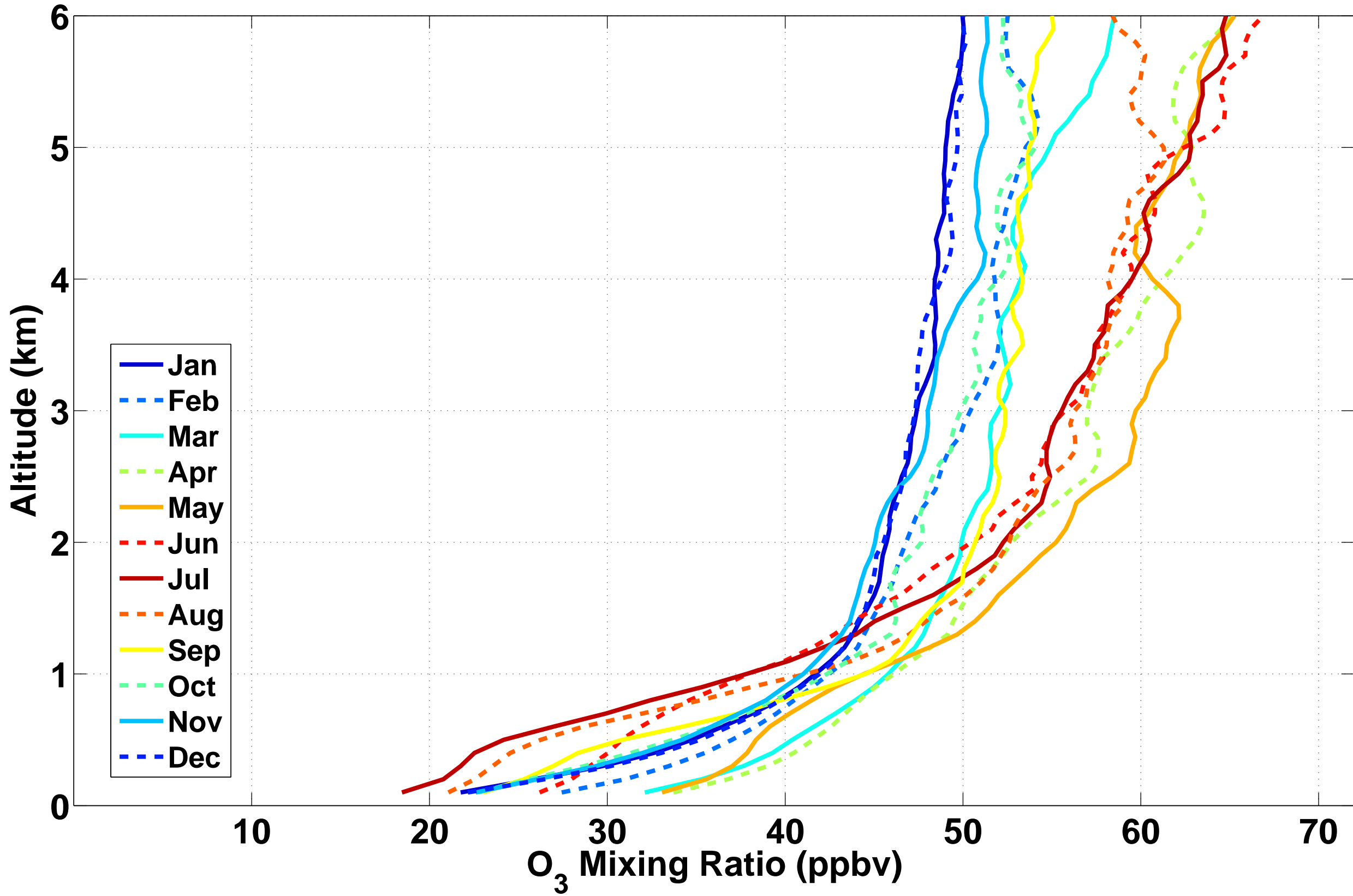
646

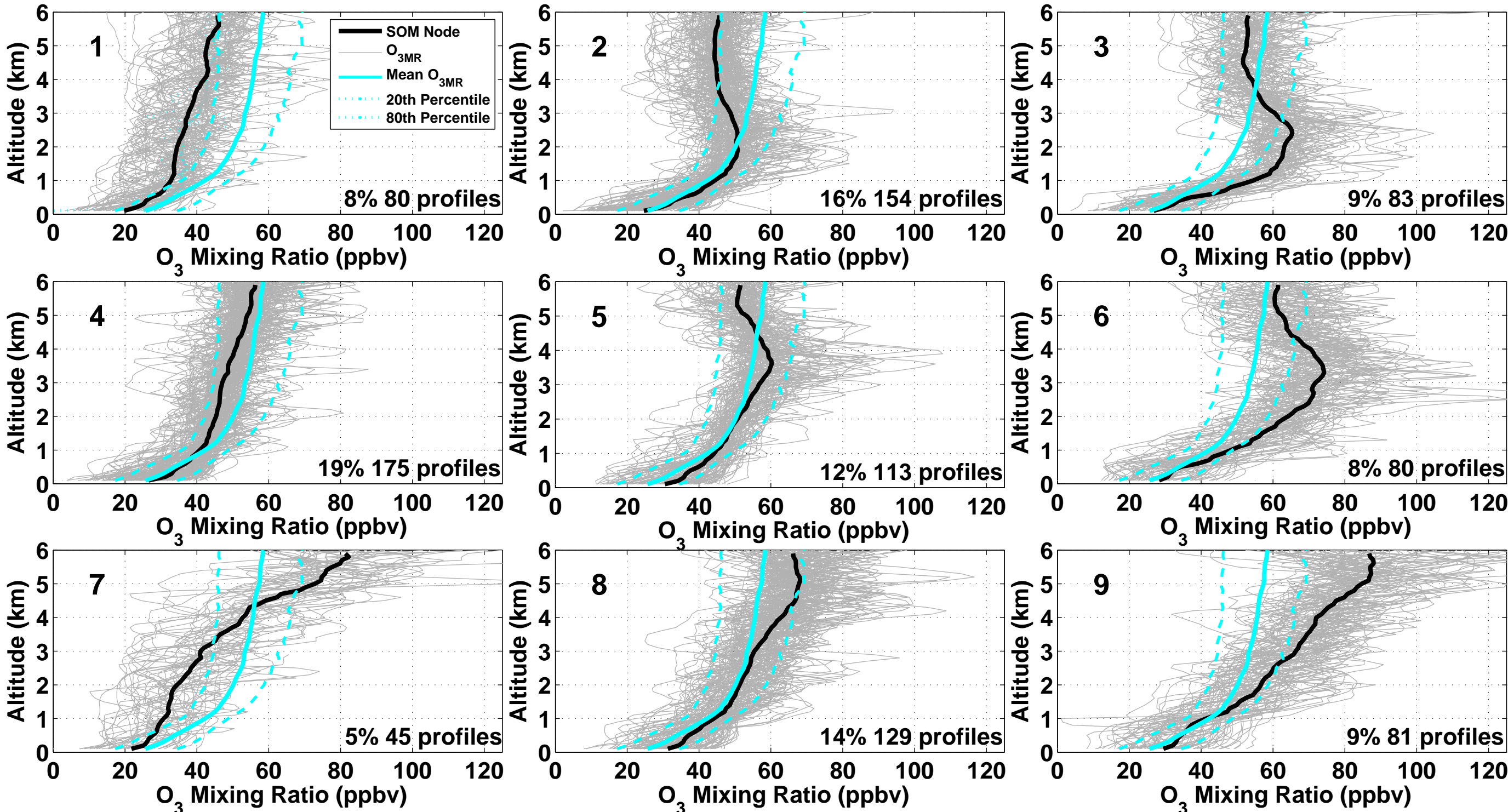


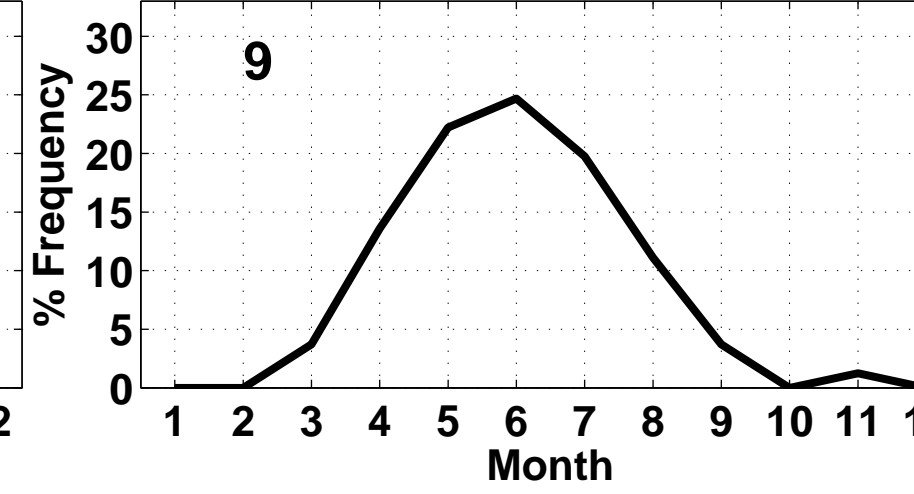
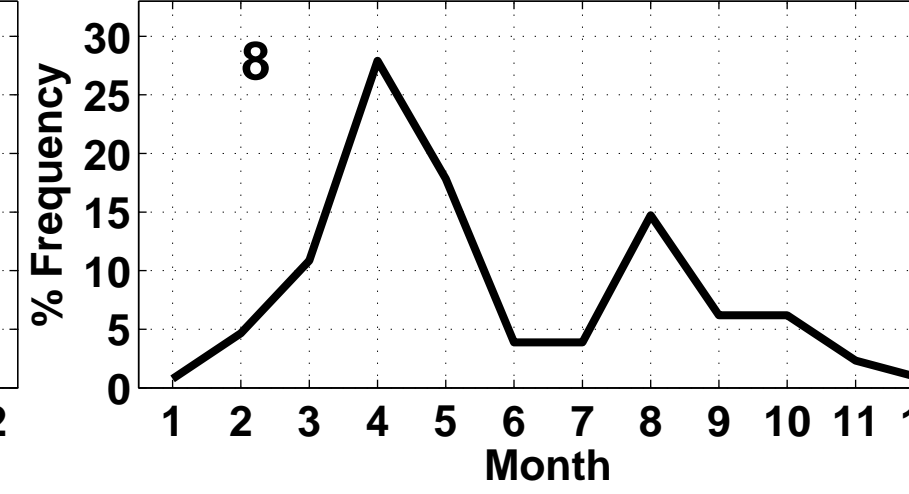
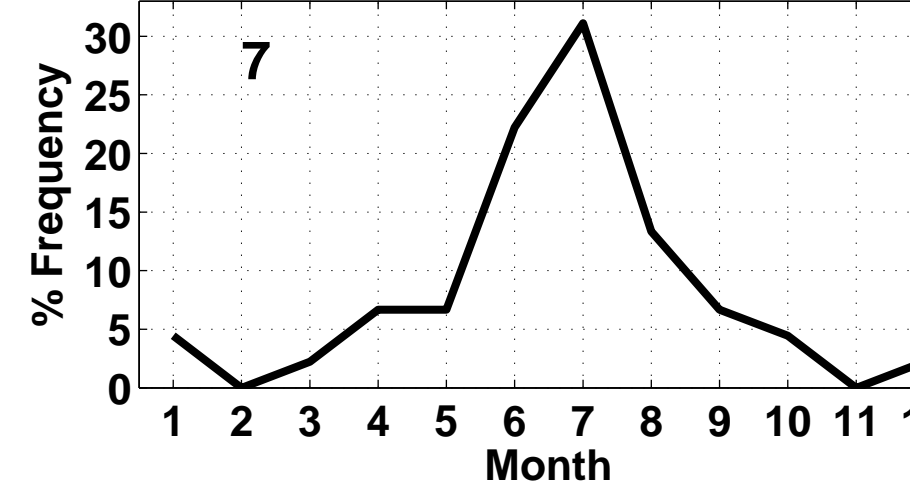
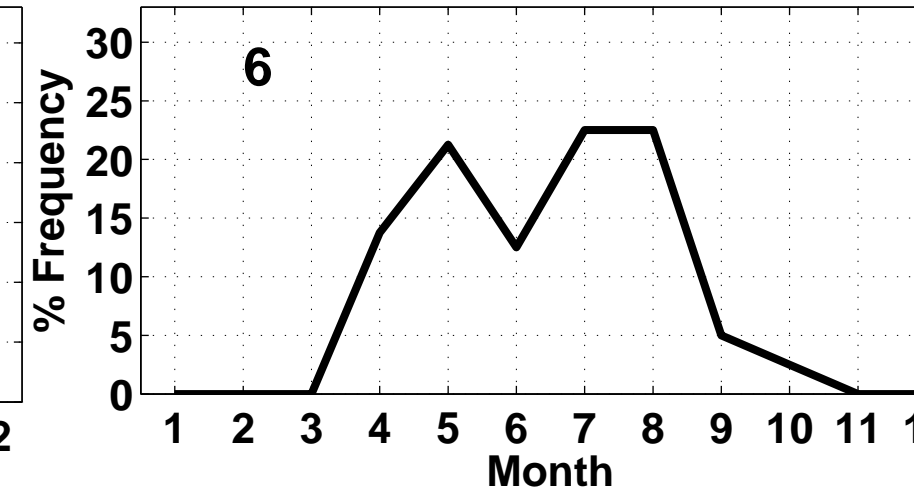
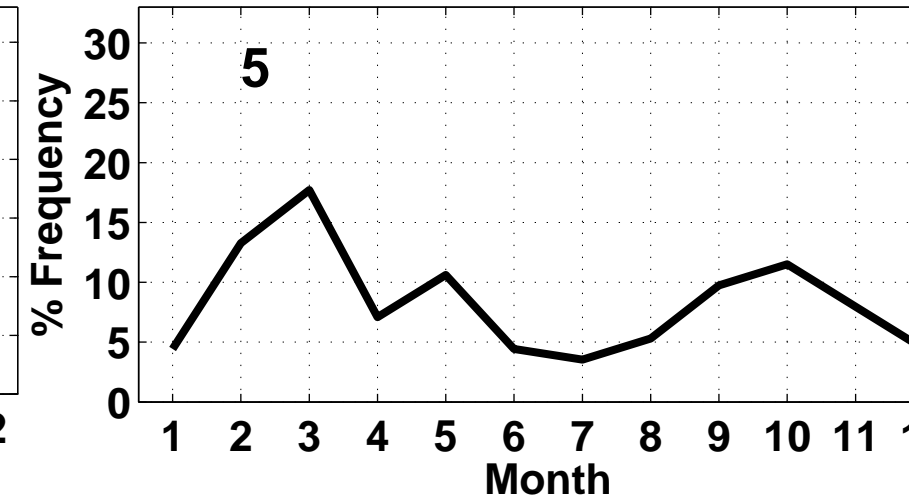
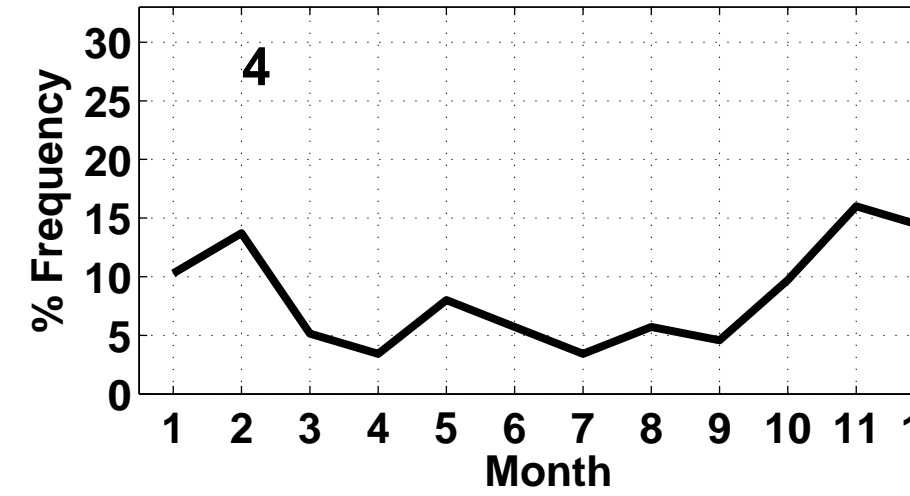
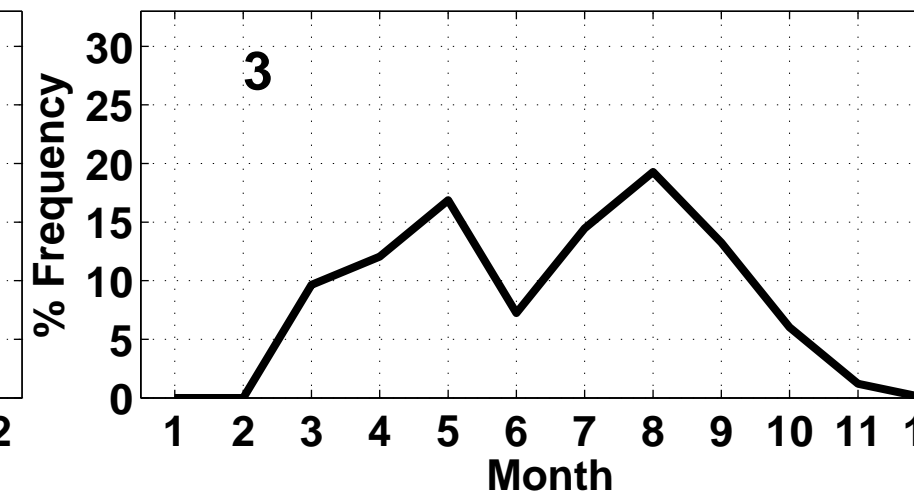
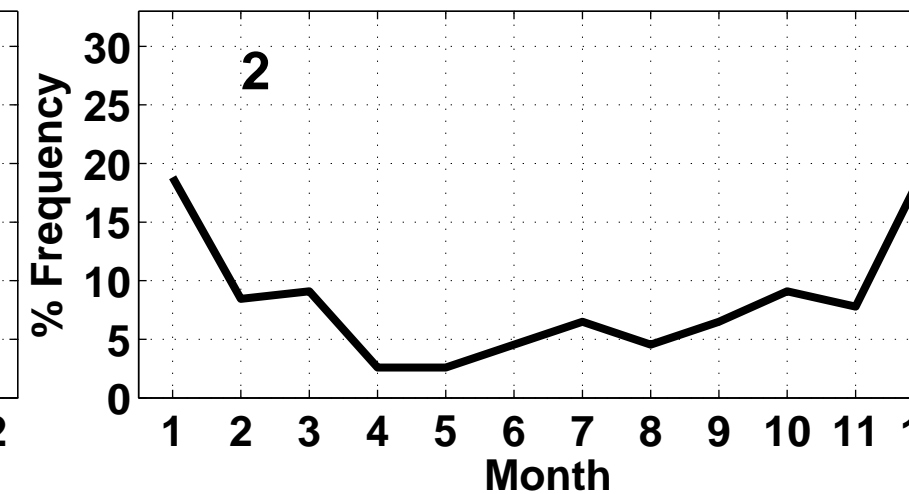
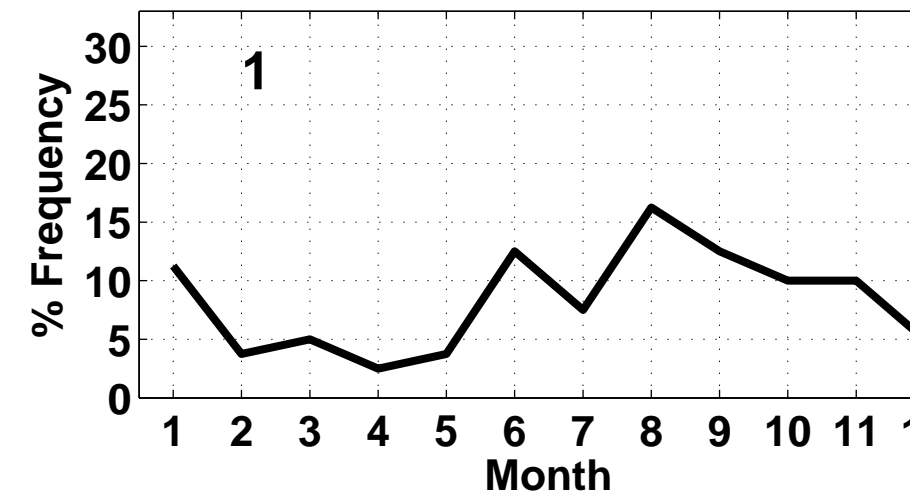
647

648 Figure A3: Contoured map of average AIRS 700 hPa O₃ anomalies from monthly climatology
 649 corresponding to each SOM node. Data are contoured every 1 ppbv from -6 to 6 ppbv. Blue
 650 colors represent negative anomalies and red colors represent positive anomalies. The green dot
 651 represents the Trinidad Head site location.

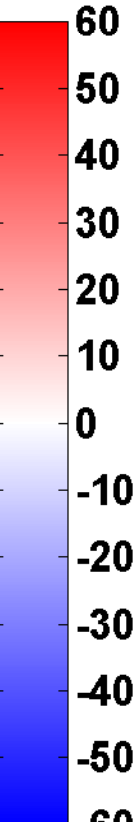
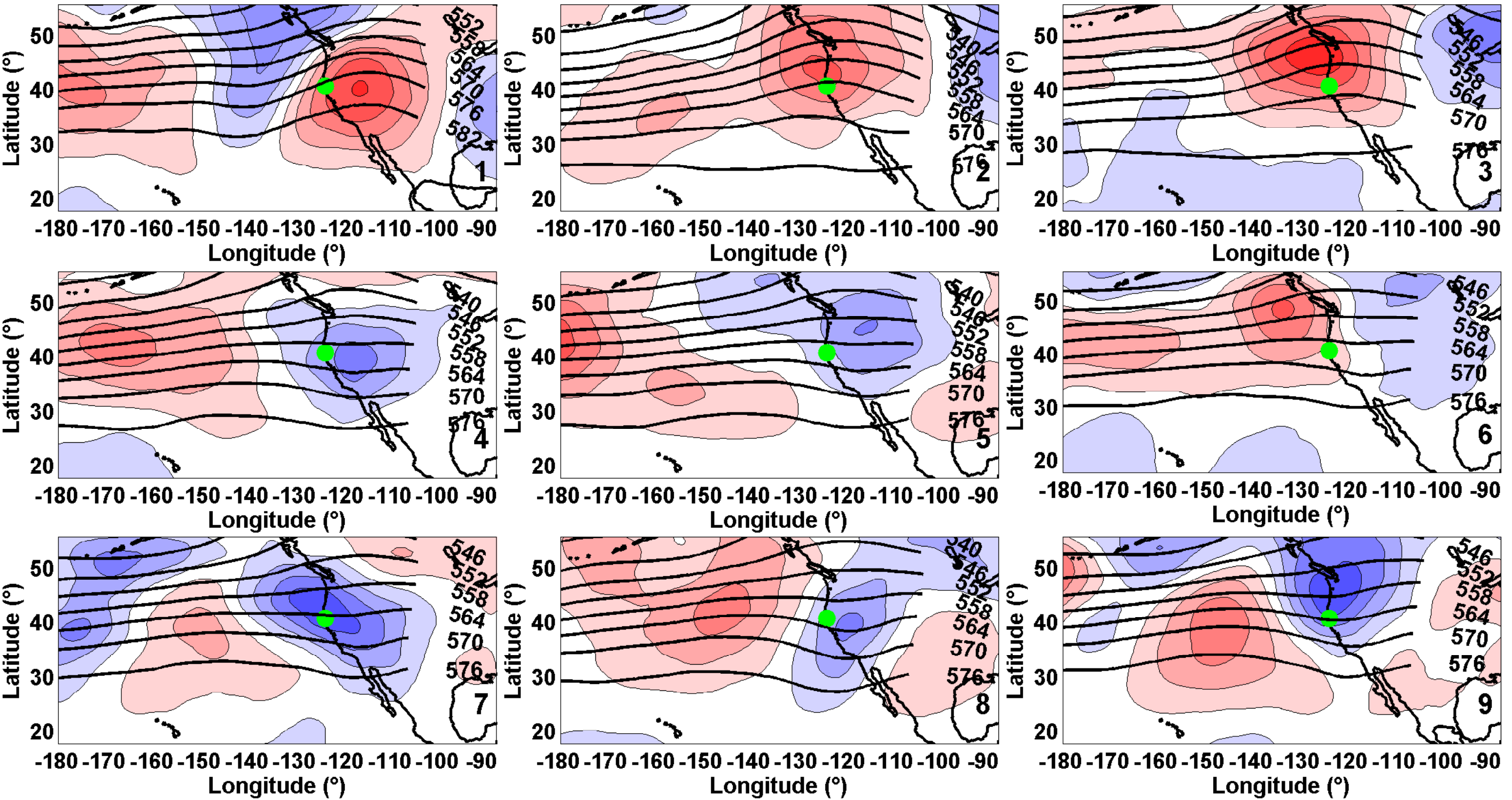
652



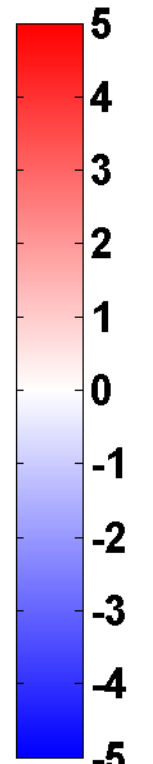
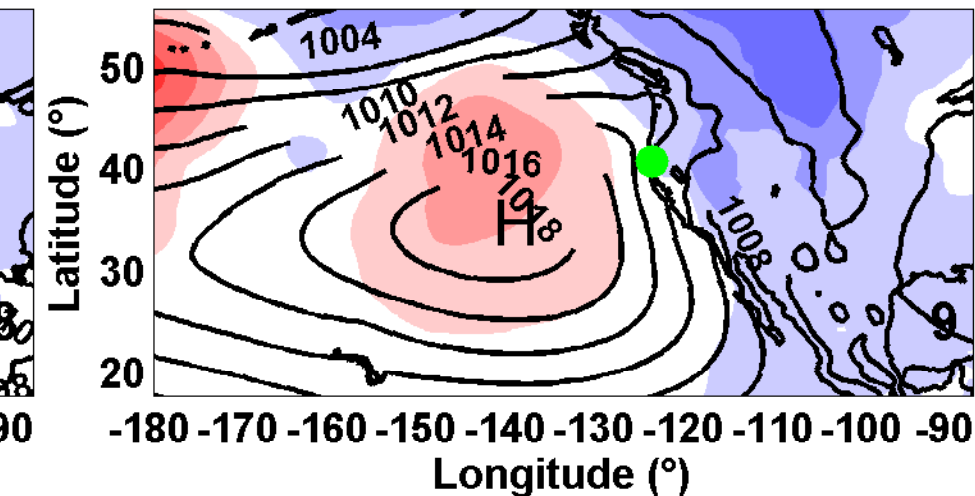
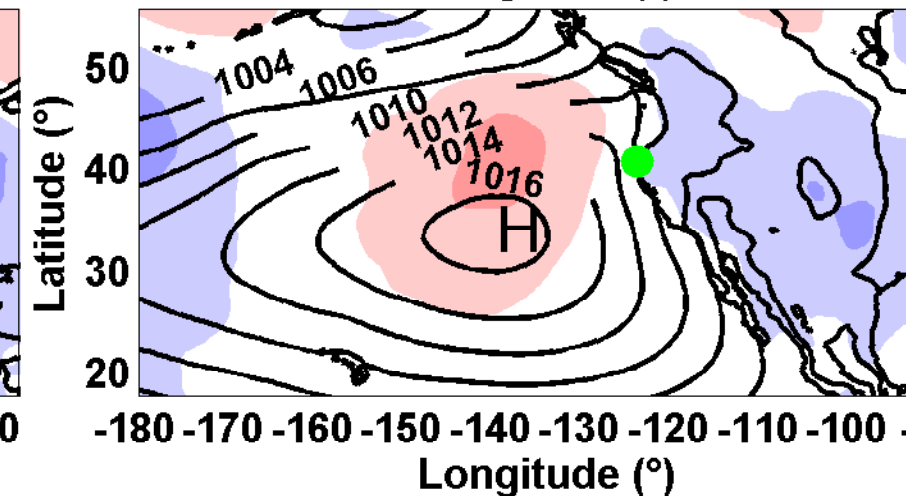
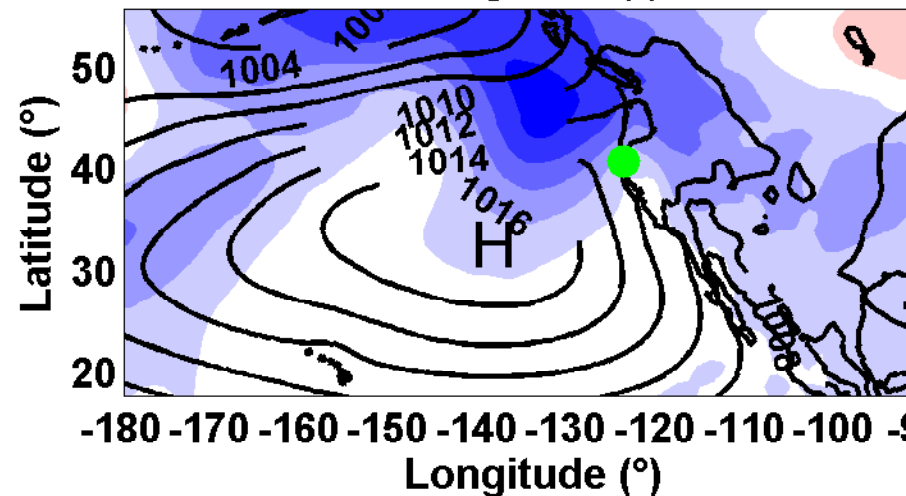
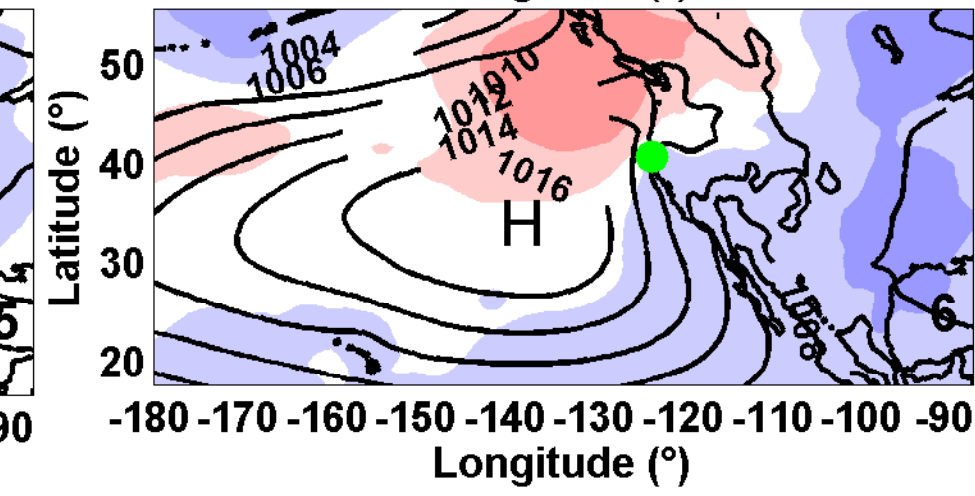
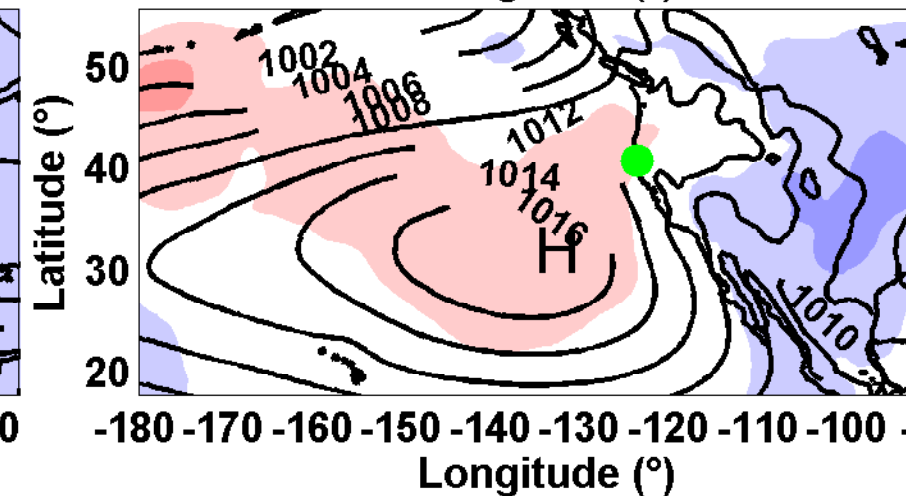
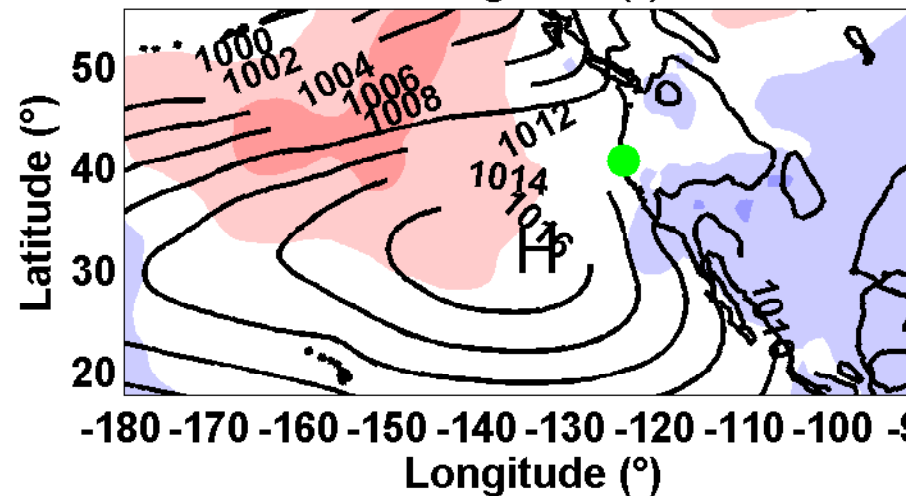
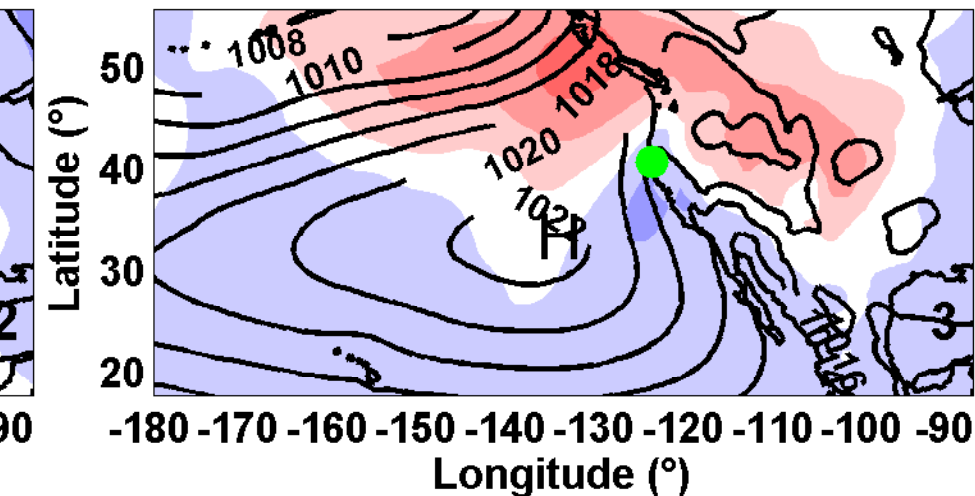
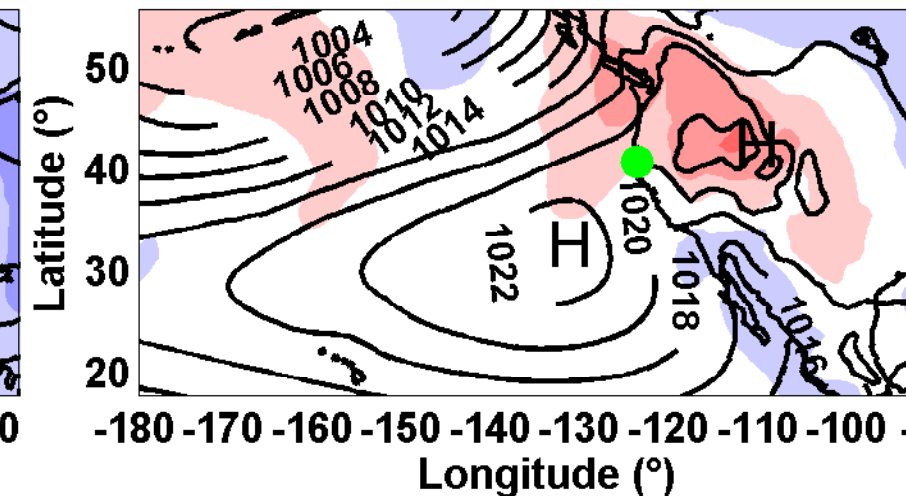
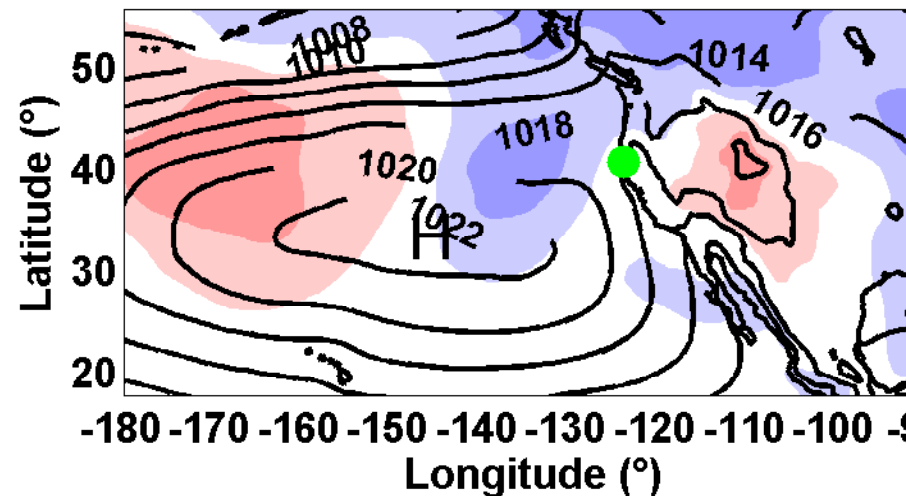


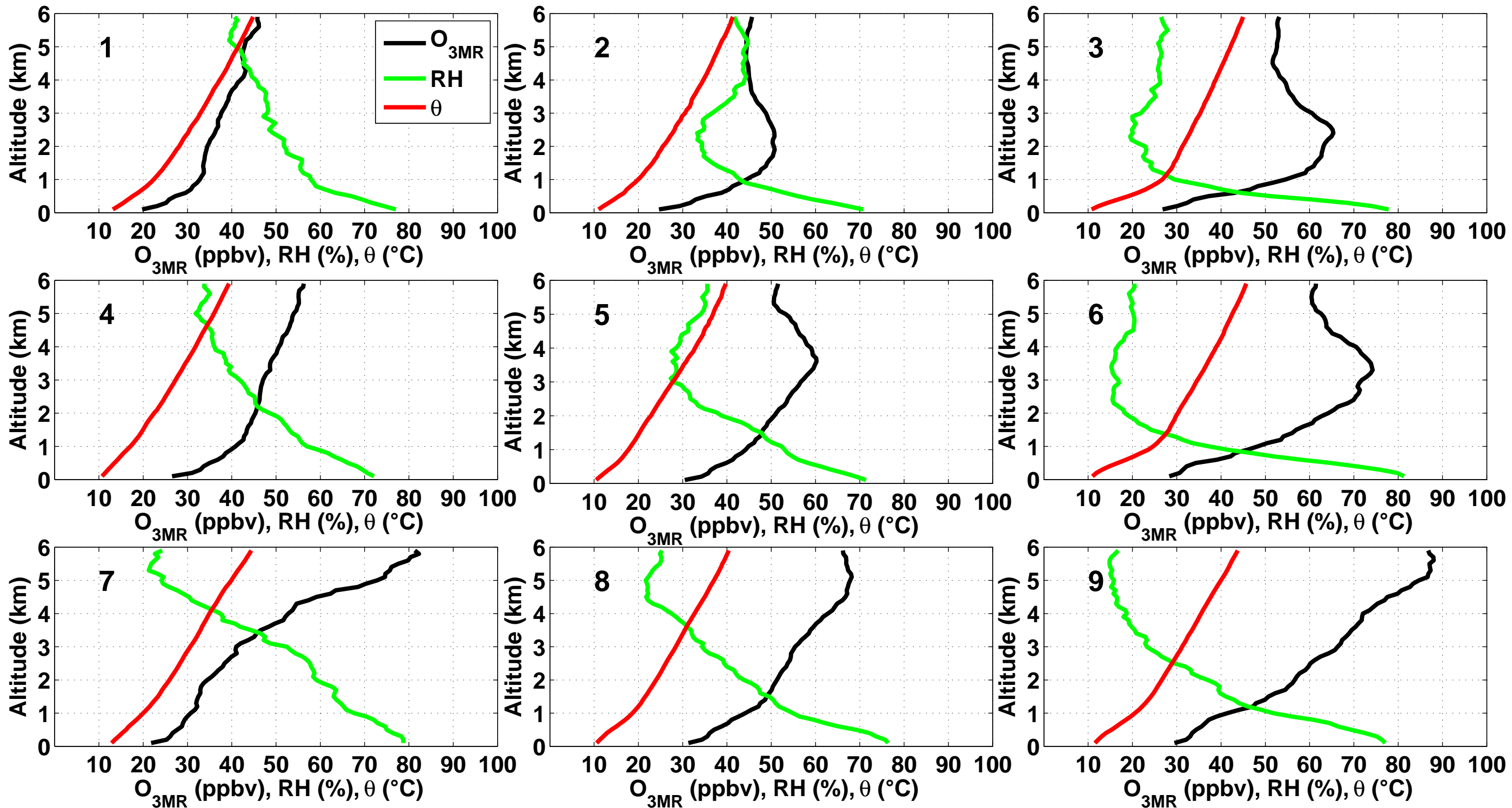


500 hPa Geopotential Height Mean (dm), Anomalies (m)

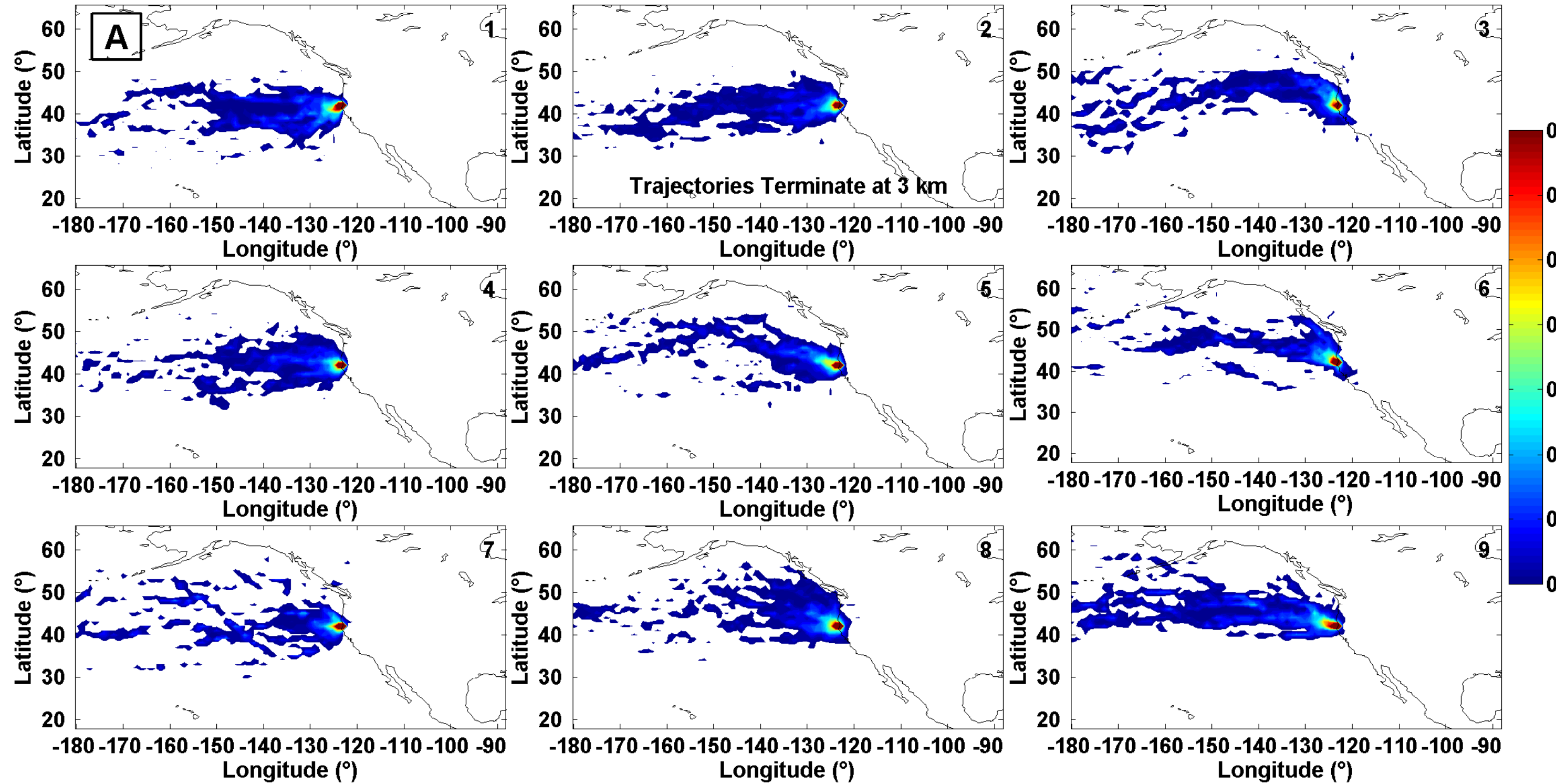


MSLP mean, Anomalies (hPa)

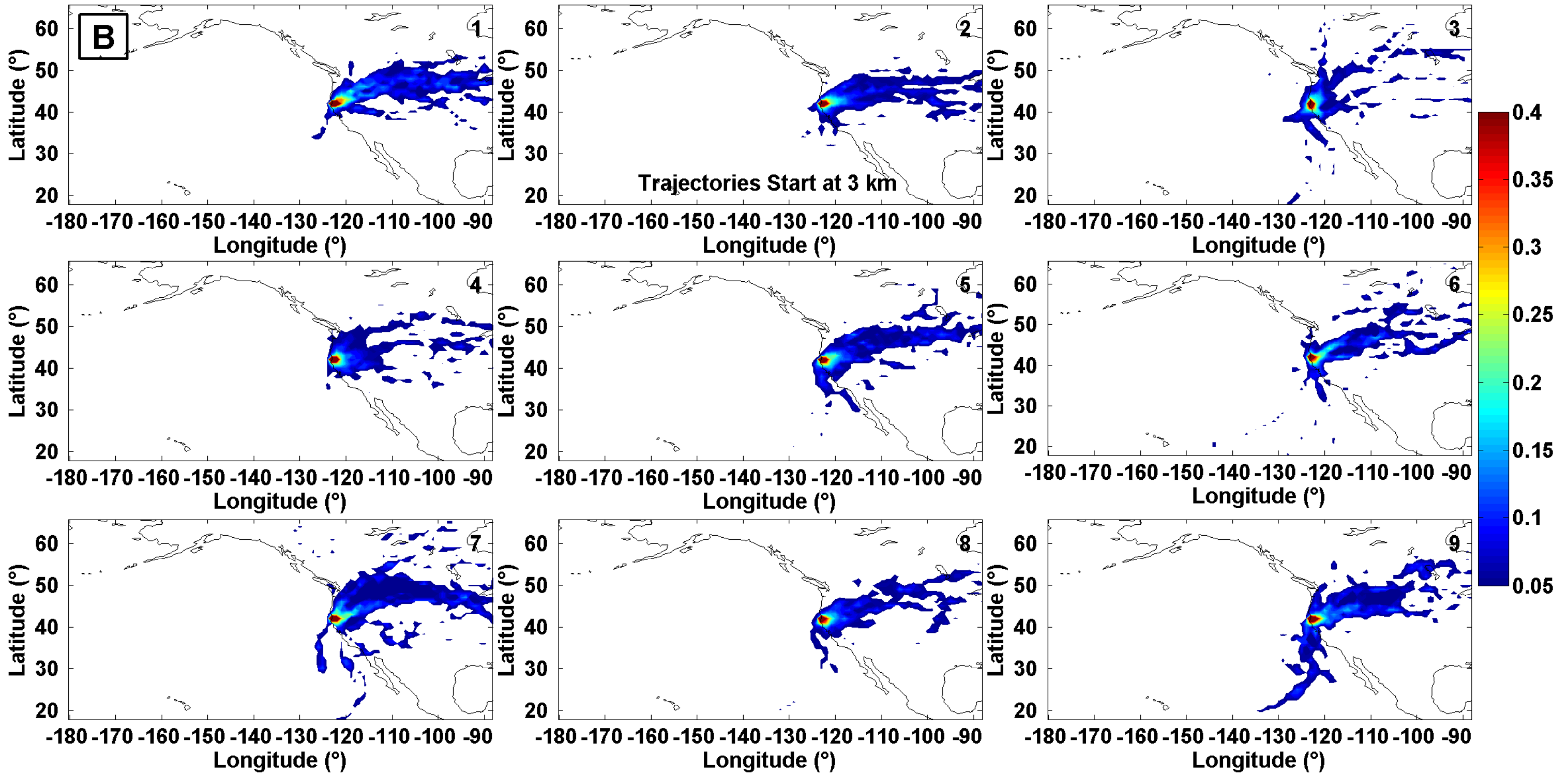


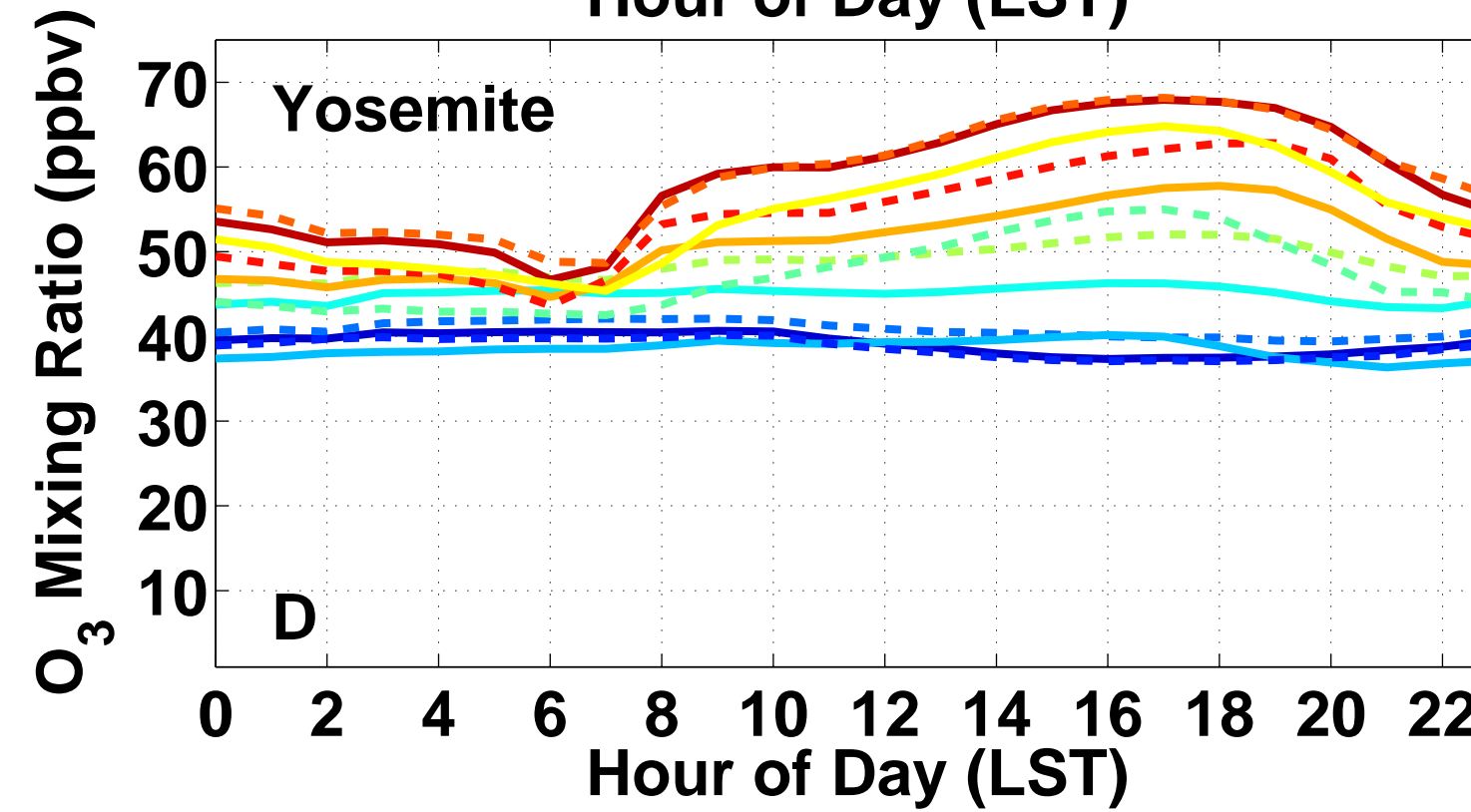
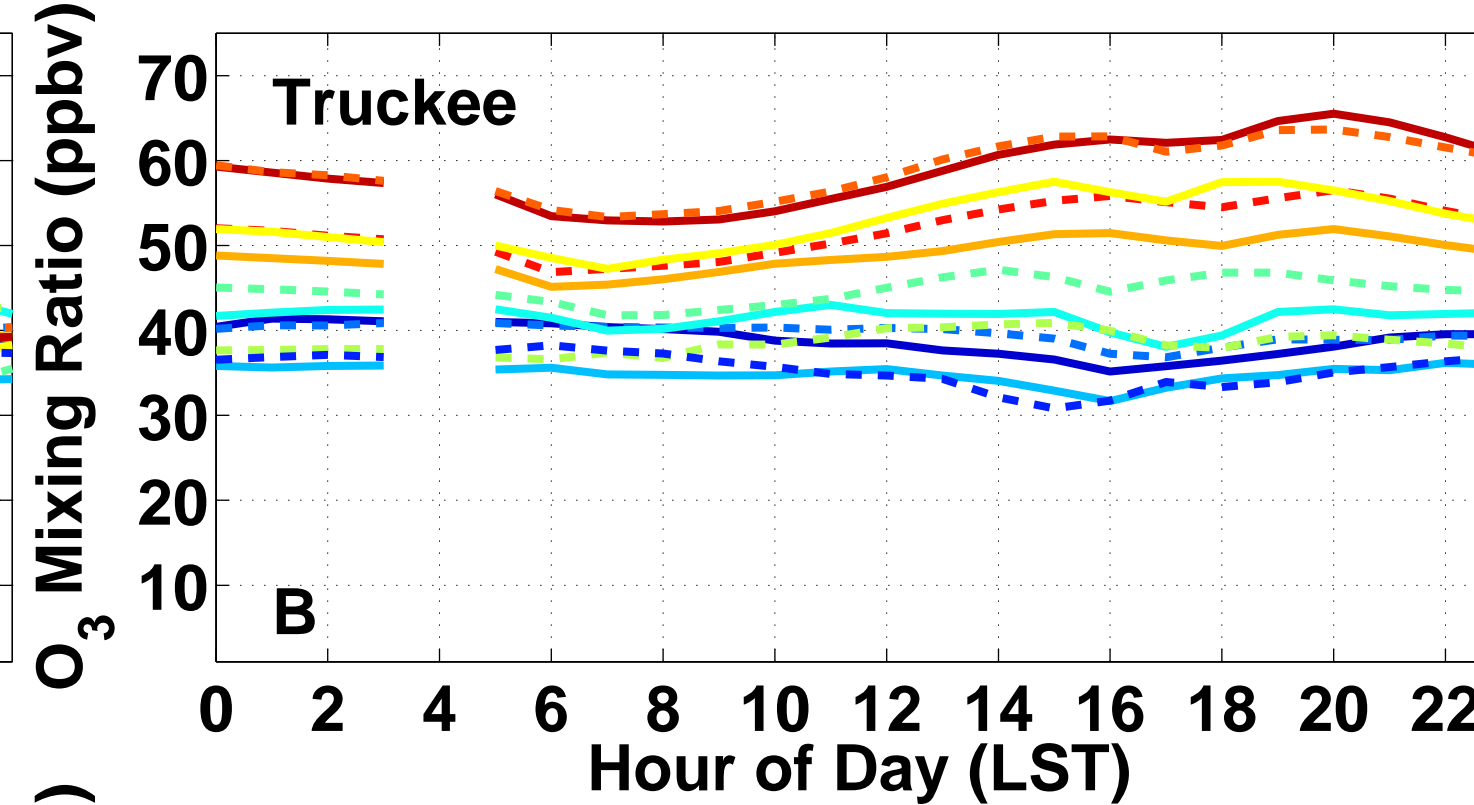
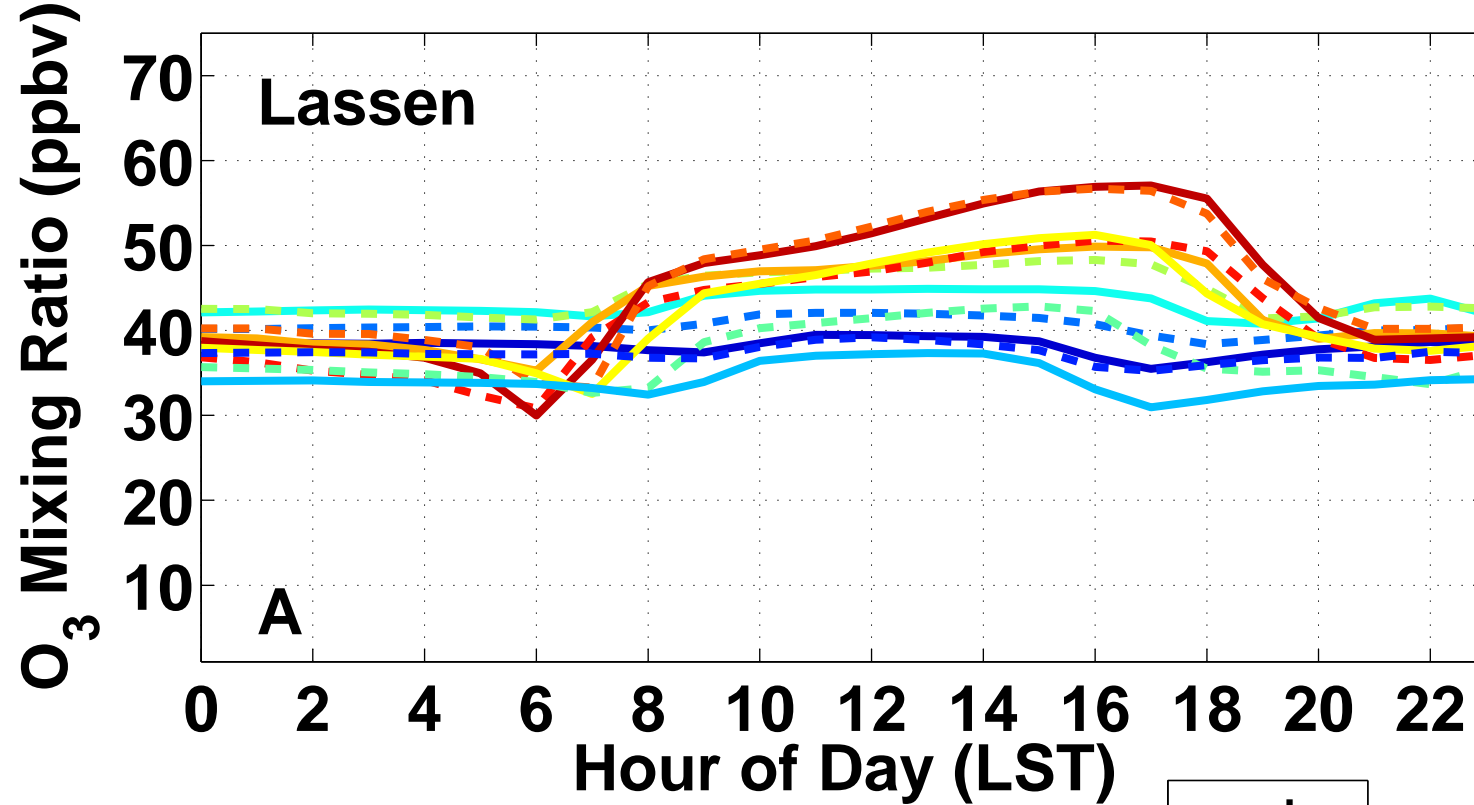


Fraction of Trajectories Passing Through $1^\circ \times 1^\circ$ Boxes

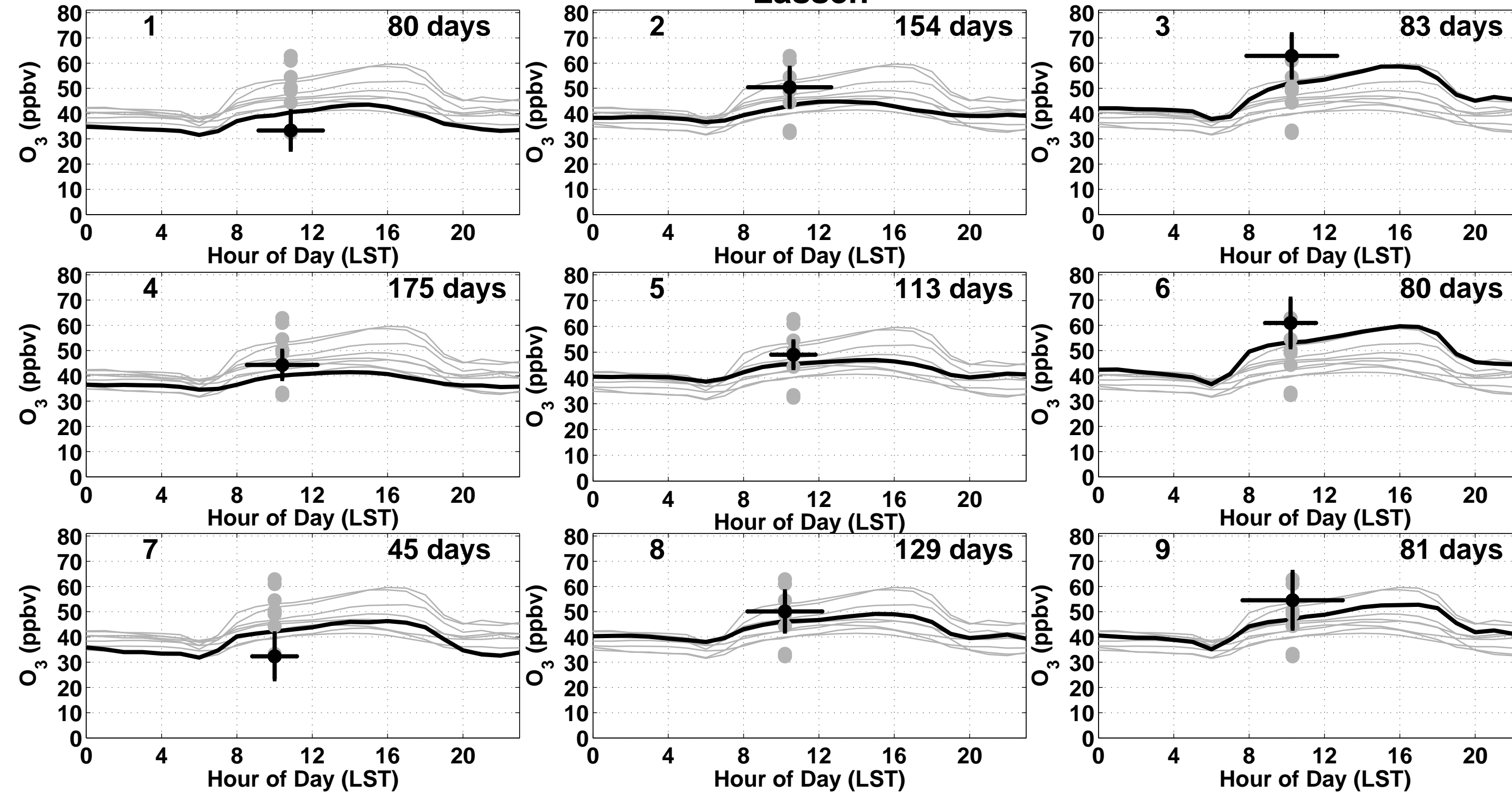


Fraction of Trajectories Passing Through $1^\circ \times 1^\circ$ Boxes

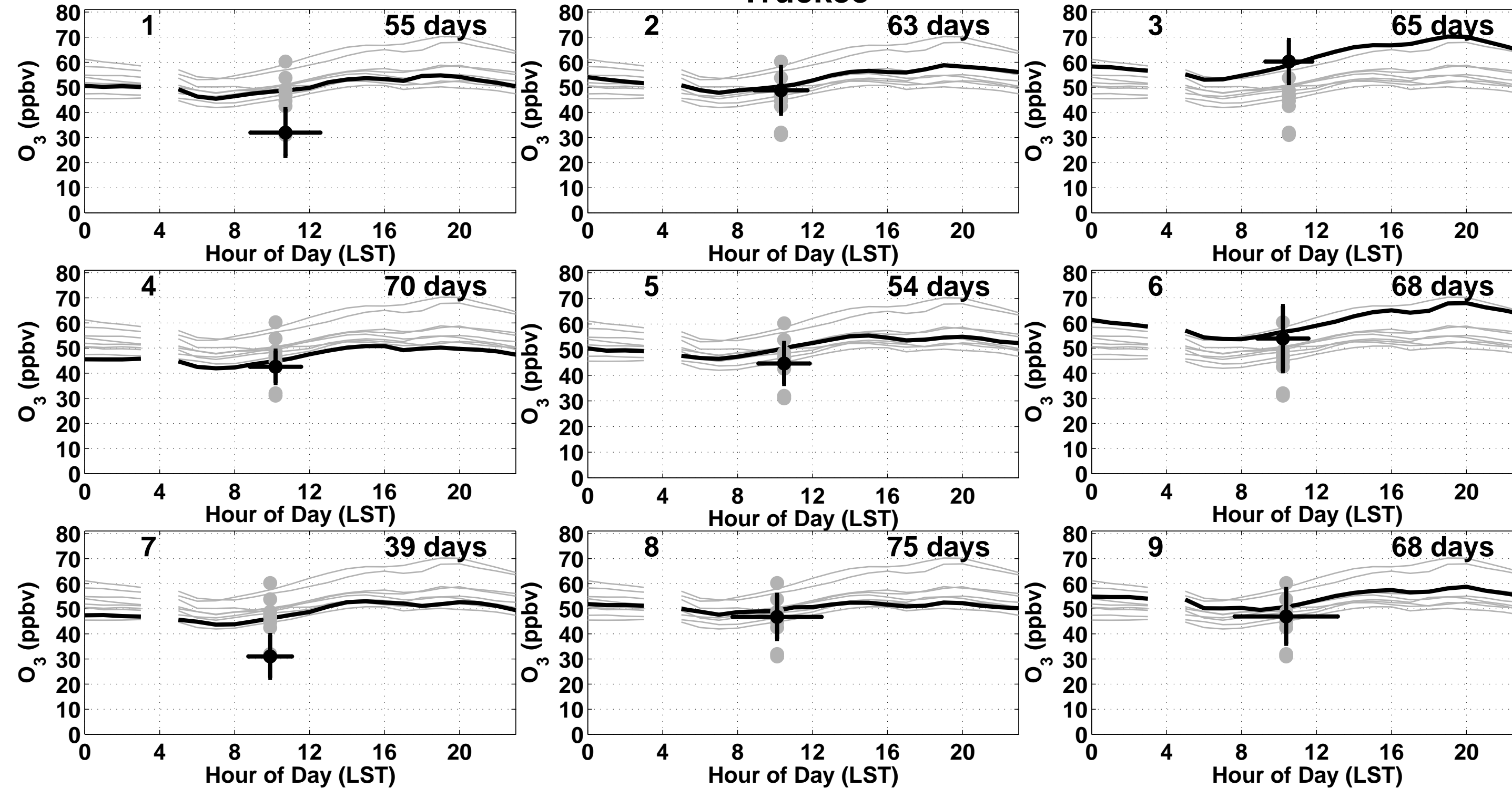




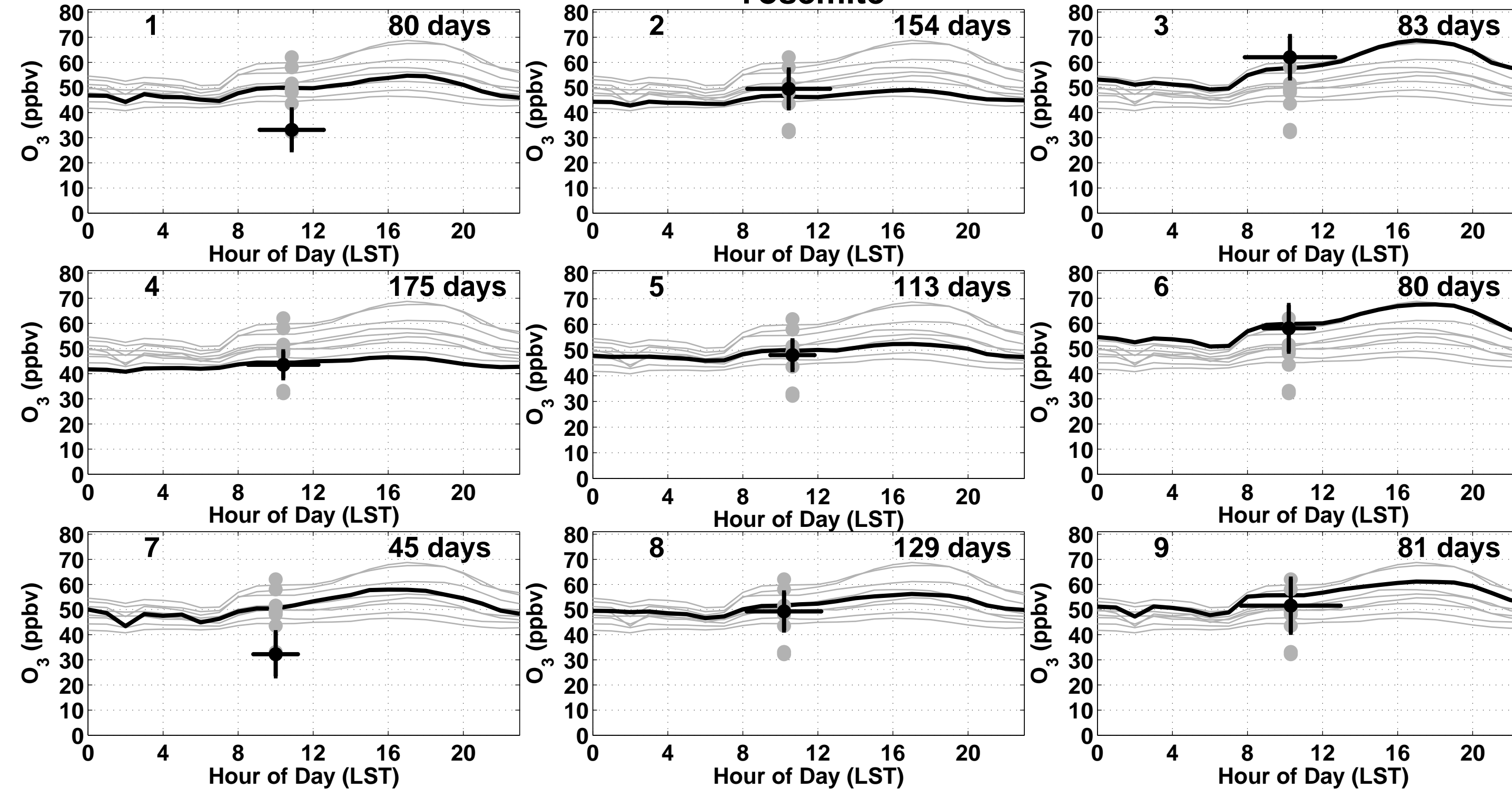
Lassen

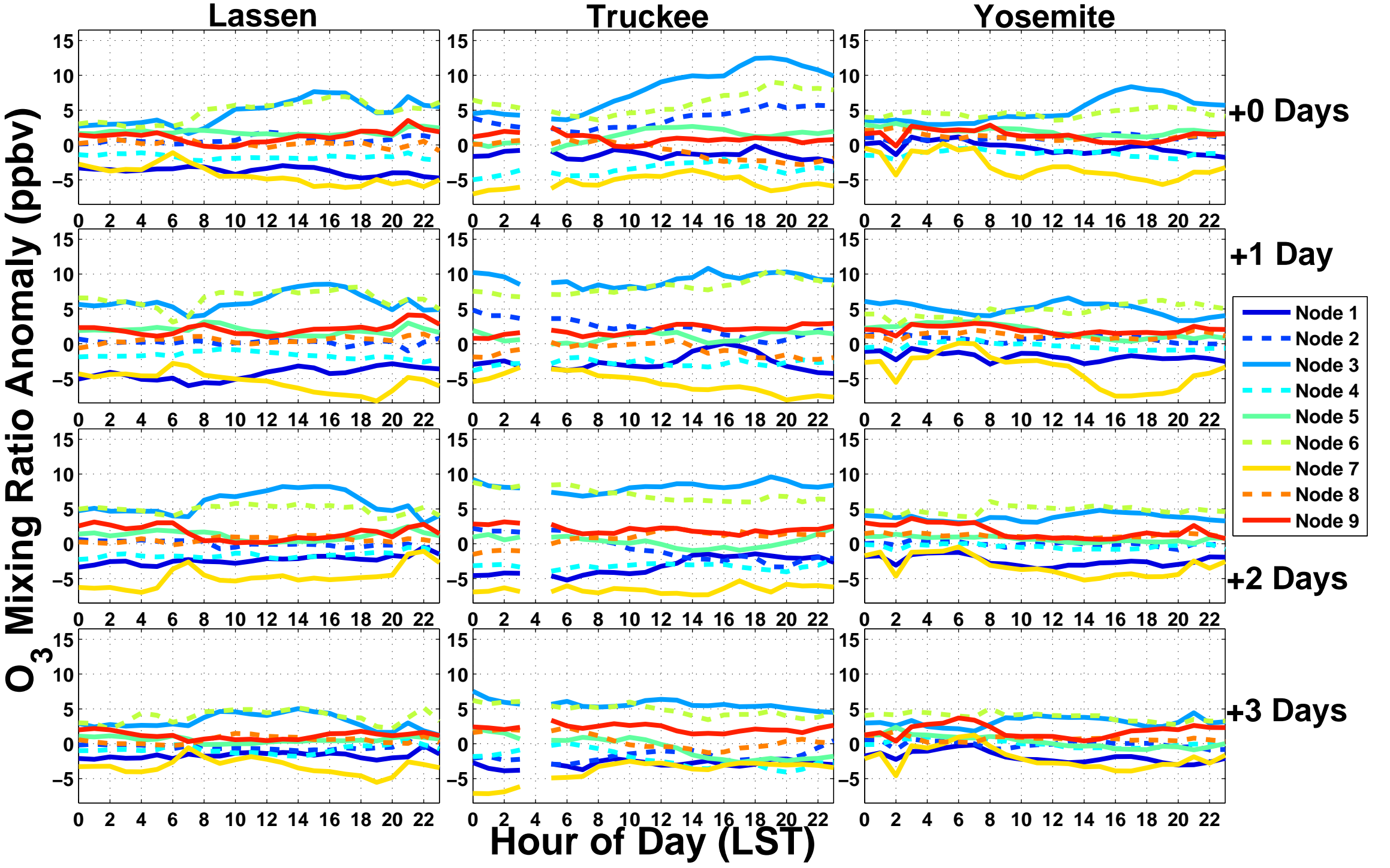


Truckee

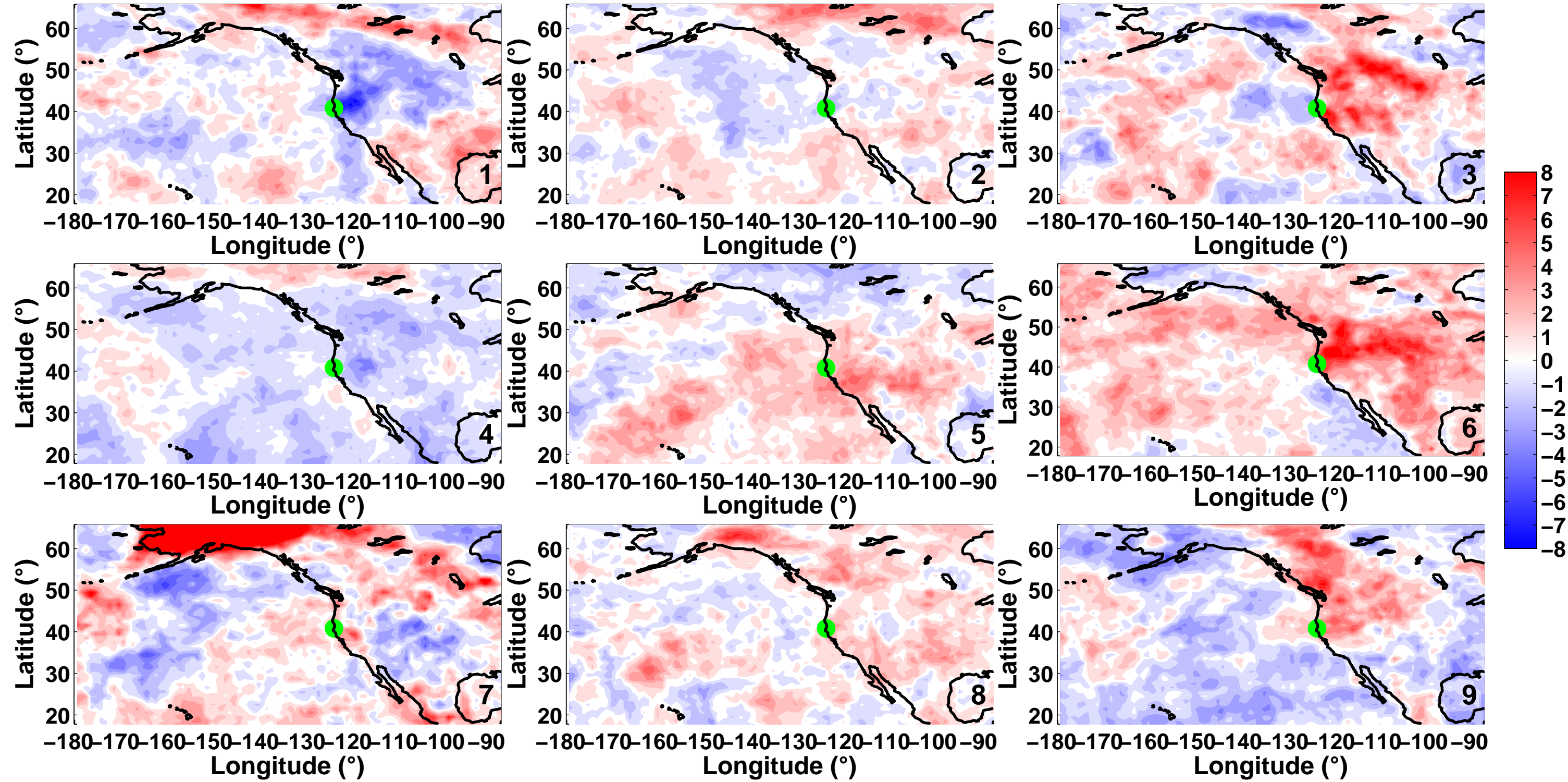


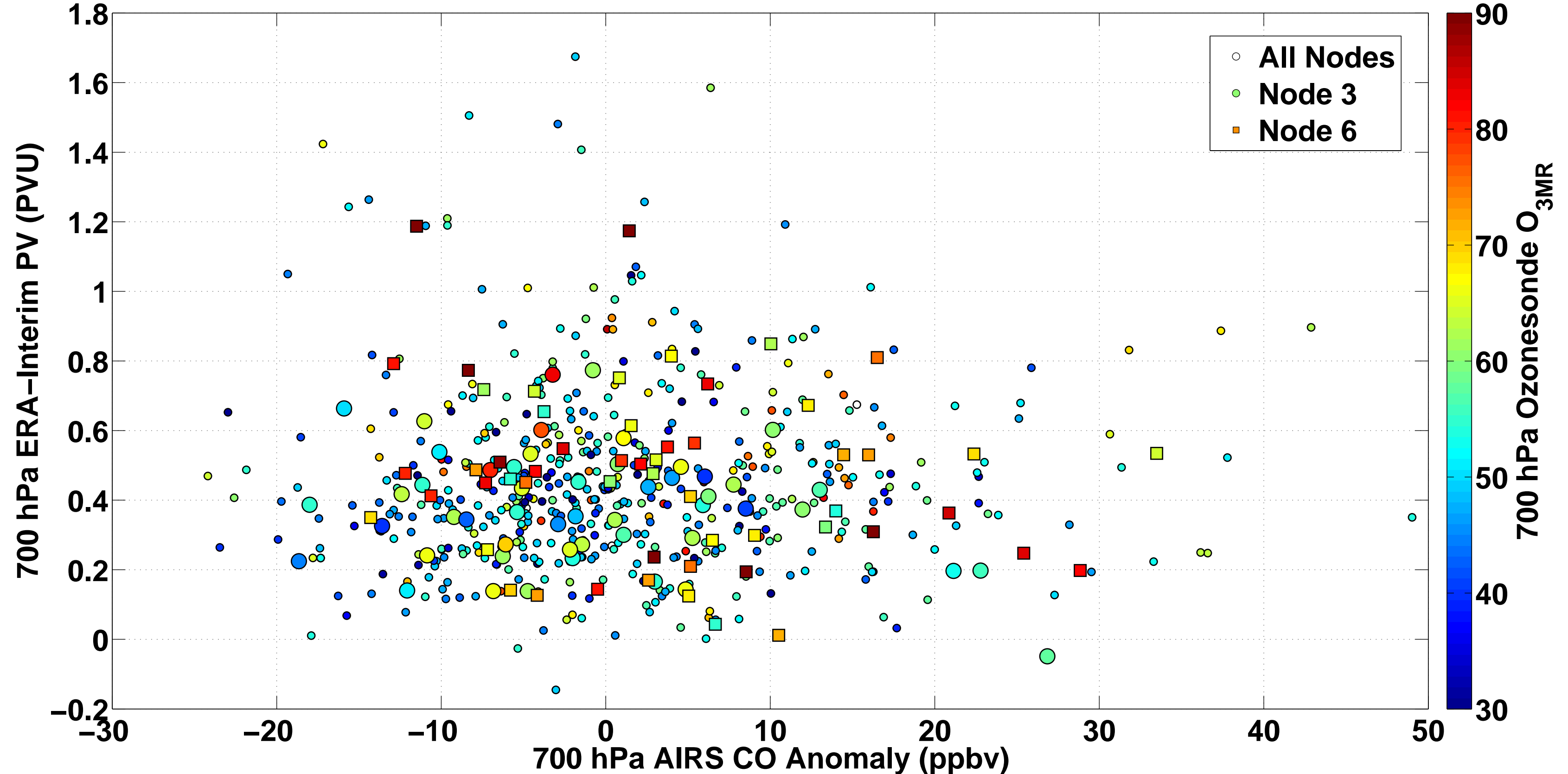
Yosemite





AIRS 700 hPa CO Anomaly (ppbv)





AIRS 700 hPa O₃ Anomaly (ppbv)

